

This work was written as part of one of the author's official duties as an Employee of the United States Government and is therefore a work of the United States Government. In accordance with 17 U.S.C. 105, no copyright protection is available for such works under U.S. Law.

Public Domain Mark 1.0

<https://creativecommons.org/publicdomain/mark/1.0/>

Access to this work was provided by the University of Maryland, Baltimore County (UMBC) ScholarWorks@UMBC digital repository on the Maryland Shared Open Access (MD-SOAR) platform.

Please provide feedback

Please support the ScholarWorks@UMBC repository by emailing scholarworks-group@umbc.edu and telling us what having access to this work means to you and why it's important to you. Thank you.

Nimbus-7 Global Cloud Climatology. Part I: Algorithms and Validation

L. L. STOWE,* C. G. WELLEMAYER,** T. F. ECK,[†] H. Y. M. YEH**,@
AND THE NIMBUS-7 CLOUD DATA PROCESSING TEAM***

*NOAA/National Environmental Satellite, Data, and Information Service, Washington, DC

**ST Systems Corporation, Lanham, Maryland

[†]Science Applications Research, Lanham, Maryland

(Manuscript received 20 November 1986, in final form 8 January 1988)

ABSTRACT

Data from the Temperature Humidity Infrared Radiometer (THIR) and the Total Ozone Mapping Spectrometer (TOMS), both aboard the Nimbus-7 satellite, are used to determine cloudiness parameters for the globe. The $11.5\ \mu\text{m}$ THIR radiances and the $0.36\ \mu\text{m}$ and $0.38\ \mu\text{m}$ TOMS reflectivities, along with concurrent surface temperature data from the Air Force 3-D nephelanalysis, are the primary data sources. They are processed by an algorithm that determines total cloud amount, cloud amount in three altitude categories, cirrus cloud, deep convective cloud, warm cloud, and the radiance of radiation emitted by the clouds and the underlying surface. The algorithm is of the bispectral threshold type, which yields two independent estimates of total cloud, one from the infrared algorithm and one from the UV reflectivity algorithm. For the daytime observations (local noon at the equator), these two independent estimates are combined to determine a composite estimate, while at night (local midnight at the equator), only the infrared threshold algorithm is used in the estimate. Quantitative validation of total cloud amount was performed by comparing the algorithm results with estimates derived by an analyst interpreting geosynchronous satellite (GOES) images, along with auxiliary meteorological data. It has been concluded that the systematic errors of the Nimbus-7 total cloud amount algorithm relative to the analyst are less than 10%, and that the random errors of daily estimates range between 7% and 16%, day or night. These empirical results are consistent with results from a theoretical sensitivity study. Qualitative validation has also been performed by making comparisons with GOES visible and infrared images for specific days. Results indicate that the TOMS cloud estimates improve the IR algorithm estimates of low cloud amount and provide for the identification of cirrus and deep convective cloud, but cloud amounts over humid tropical regions tend to be overestimated even with the use of TOMS. These results suggest that the spatial and temporal characteristics of daily and monthly averaged global cloud cover, including cirrus and deep convective cloud types, which are presented in Part II, are generally well represented by the Nimbus-7 dataset, which covers a six-year period from April 1979 to March 1985.

1. Introduction

Knowledge of the global distribution of cloud amount and height over many years is important for studies related to the Earth's radiation budget, climate change, and general circulation modeling (WMO 1978; WCRP 1982). Determining the relationships between the Earth's radiation budget and cloud parameters and the effects these relationships have on climate has been the subject of numerous recent investigations, both theoretical and empirical (e.g., Wetherald and Manabe

1980; Gordon et al. 1984; Hartmann and Short 1980; Ohring et al. 1981; Cess et al. 1982).

However, the validity of conclusions from these studies has been questioned because of inadequacies in the observational data used to either validate the theoretical relationships between clouds and radiation or to derive the relationships between the Earth's radiation budget components and cloud parameters. The Nimbus-7 satellite, launched on 24 October 1978, offers, for the first time, a concurrent cloud and radiation budget dataset that can be used to study these important scientific questions. The radiation budget observations are derived from the Earth Radiation Budget (ERB) experiment (Jacobowitz et al. 1984), and the cloud data are computed by using radiation measurements from THIR (Hwang 1982), and TOMS (Heath et al. 1978). Analyses of surface temperature and snow/ice cover archived by the Air Force from their Three-Dimensional Nephelanalysis program (Fye 1978) are also used. These datasets were added to the THIR data when the results of an initial attempt at deriving cloud parameters from an infrared-only algorithm using THIR data

* Present affiliation: Caelum Research Corporation, Silver Spring, MD 20906.

*** P. H. Hwang, Former Team Manager, H. L. Kyle, Present Team Manager, NASA/GSFC; L. L. Stowe, Principal Scientist, P. P. Pellegrino, NOAA/NESDIS; P. K. Bhartia, C. S. Long, C. G. Wellemeyer, H. Y. M. Yeh, ST Systems Corporation; T. F. Eck, Science Applications Research.

Corresponding author address: Dr. H. L. Kyle, NASA, Goddard Space Flight Center, Greenbelt, MD 20771.

and climatological temperature information were found to have large uncertainties (Stowe 1984).

This paper reports on the validation of results from the improved version of the Nimbus-7 cloud retrieval algorithm. It is shown, both quantitatively and qualitatively, that when concurrent surface temperatures and errors due to variation in water vapor attenuation, horizontal temperature gradients, and partially cloudy radiometer fields-of-view are incorporated into the infrared algorithm, and when UV reflectance measurements from TOMS are used to independently estimate total cloud amount, the accuracy of the estimated cloud parameters is greatly improved. The TOMS reflectance measurements are particularly useful for the detection of low clouds, which have a small thermal contrast with the surface and are, therefore, difficult to detect with only infrared data. Also, both ocean and land surface reflectivities are uniformly low in the UV, which is not the case in the visible part of the spectrum, thus simplifying the procedures used for cloud detection with reflectance data. THIR clouds together with TOMS reflectances are analyzed to identify areas covered only with thin cirrus or deep convective clouds and to estimate their amount.

Six years of continuous cloud parameter observations have been produced from Nimbus-7 data, beginning with 1 April 1979, the date when the Air Force surface temperature analysis became available. This six-year period is of particular interest for climate related studies because it contains the First Global GARP Experiment (FGGE), the eruption of the El Chichón volcano in the spring of 1982, and the 1982/83 El Niño/Southern Oscillation (ENSO) event, considered to be one of the largest climate perturbations in recent history. The International Satellite Cloud Climatology Project (ISCCP), established by the World Climate Research Program (WCRP) (Schiffer and Rossow 1983), and NASA's ERBE program (Barkstrom 1984), together with the Nimbus-7 ERB and CLOUD programs, should extend the period covered by concurrent cloud and radiation budget datasets to at least July 1988, providing the climate community with almost ten consecutive years of these important observations.

Section 2 describes the datasets used in estimating the cloud parameters. The methods used to compute cloud amount at three different altitudes are described in section 3. Section 4 presents a discussion of the validation results, and the conclusions are presented in section 5. The overall validation of the Nimbus-7 cloud dataset will be presented in two parts. This paper, Part I, describes the data sources, the cloud algorithm, and the specific validation of both. Part II, which will follow, will describe spatial and temporal characteristics of the dataset cloud types and associated $11.5\ \mu\text{m}$ radiances during the first data year. There, comparison will be made with older global cloud datasets (London 1957; Berlyand and Strokina 1980; Hughes and Henderson-Sellers 1985) and with other cloud data sources such

as Hahn et al. (1982, 1984). In general, quantitative problems are addressed in this paper, while some questions, that can best be discussed qualitatively, will be reserved for Part II.

2. Data

The Nimbus-7 satellite is in a sun-synchronous orbit inclined 99.3° to the equator, with a period of 103.9 minutes. The satellite's altitude is approximately 955 km, and it performs 13.9 orbits per day. It crosses the equator near local noon on the ascending node (AN) traveling from south to north, and near local midnight on the descending node (DN) going south. Between 45°N and 45°S latitude, observations are taken within an hour of local noon during the day and within an hour of local midnight at night. Near the poles, the satellite moves parallel to the 80th latitude and quickly traverses the remaining local time zones before heading back toward the equator. The subsatellite point never goes beyond latitude 80.7° so that while the scanning sensors view the poles, they never do so near nadir. The Nimbus-7 products are normally produced and stored on a separate ascending node and descending node basis. For most of the globe, these can accurately be described as local noon (AN), and local midnight (DN) data products, or loosely as day and night products. We will normally refer to them as AN or DN measurements or products.

a. Temperature humidity infrared radiometer (THIR) data

The Nimbus-7 THIR is designed and operated identically to the ones flown on Nimbus 4, 5 and 6, except that the measurements are digitized aboard the spacecraft. The two-channel scanning radiometer measures Earth radiation from two spectral bands during day and night. A 10.5 to $12.5\ \mu\text{m}$ ($11.5\ \mu\text{m}$) window channel provides an image of the cloud cover and temperatures of the cloud, land, and ocean surfaces. A 6.5 to $7.0\ \mu\text{m}$ ($6.7\ \mu\text{m}$) channel provides information on the moisture and possibly the cirrus cloud content of the middle and upper troposphere (Fritz and Rao 1967). The ground resolution at the sub-satellite point is 6.7 kilometers for the $11.5\ \mu\text{m}$ channel and 20 kilometers for the $6.7\ \mu\text{m}$ channel. At a nadir angle of 50° , where interorbit coverage is achieved at the equator, the ground resolution is $13 \times 24\ \text{km}$ and $36 \times 75\ \text{km}$ for the $11.5\ \mu\text{m}$ and $6.7\ \mu\text{m}$ channels, respectively.

The radiometer scan mirror, which provides the necessary scan motion to produce nearly contiguous cross-track scanning, continuously rotates the FOV of the detector through 360 degrees in a plane normal to the spacecraft velocity vector at 48 rpm. In sequence, the detector views the in-flight blackbody calibration target (which is part of the radiometer housing), outer space, Earth, outer space and returns again to view the

TABLE 1. THIR instrument performance.

Parameter Description	11.5 micron	6.7 micron
Wavelength band of operation [half-power points (micron)]	10.5–12.5	6.5–7.0
FOV dimension: parallel to satellite track × perpendicular to satellite track (km)	Nadir = 0°	
	6.7 × 6.7	20 × 20
	Nadir = 50°	
	13 × 24	36 × 75
Noise equivalent temperature: differential at indicated scene temperature	1.5° @ 185 K 0.28° @ 300 K	5.0° @ 185 K 0.26° @ 300 K
Digitization temperature: differential at indicated scene temperature	2.8° @ 185 K 0.5° @ 300 K	5.7° @ 185 K 0.15° @ 300 K

radiometer housing. This sequence allows for in-flight calibration of THIR by using the space measurement and the calibration target measurement, along with the assumption of linear instrument response. Monitoring

of the target temperature over the entire six-year dataset indicates that the calibration system is stable, and capable of maintaining the accuracy quoted in Table 1. A more detailed description of the instrument is available in the THIR Data User's Guide (Hwang 1982).

A global map of the THIR 11.5 μm equivalent blackbody temperatures for 5 August 1979, is shown in Fig. 1. A discussion of this figure in comparison with an ultraviolet reflectivity map is given below in section 2b.

b. TOMS data

The TOMS instrument is a single monochromator whose field of view (FOV) is scanned perpendicularly to the orbital plane through the satellite subpoint by a rotating mirror. The UV backscattered radiation is measured at six wavelengths from 0.313 to 0.380 μm sequentially in three-degree steps along the scan, which spans 51 degrees to either side of nadir (Heath et al. 1978). The 0.360 and 0.380 μm wavelengths, which are not absorbed by the ozone, are included to provide an estimate of the UV reflectivity of a surface below or within the atmosphere. Measurements are also made

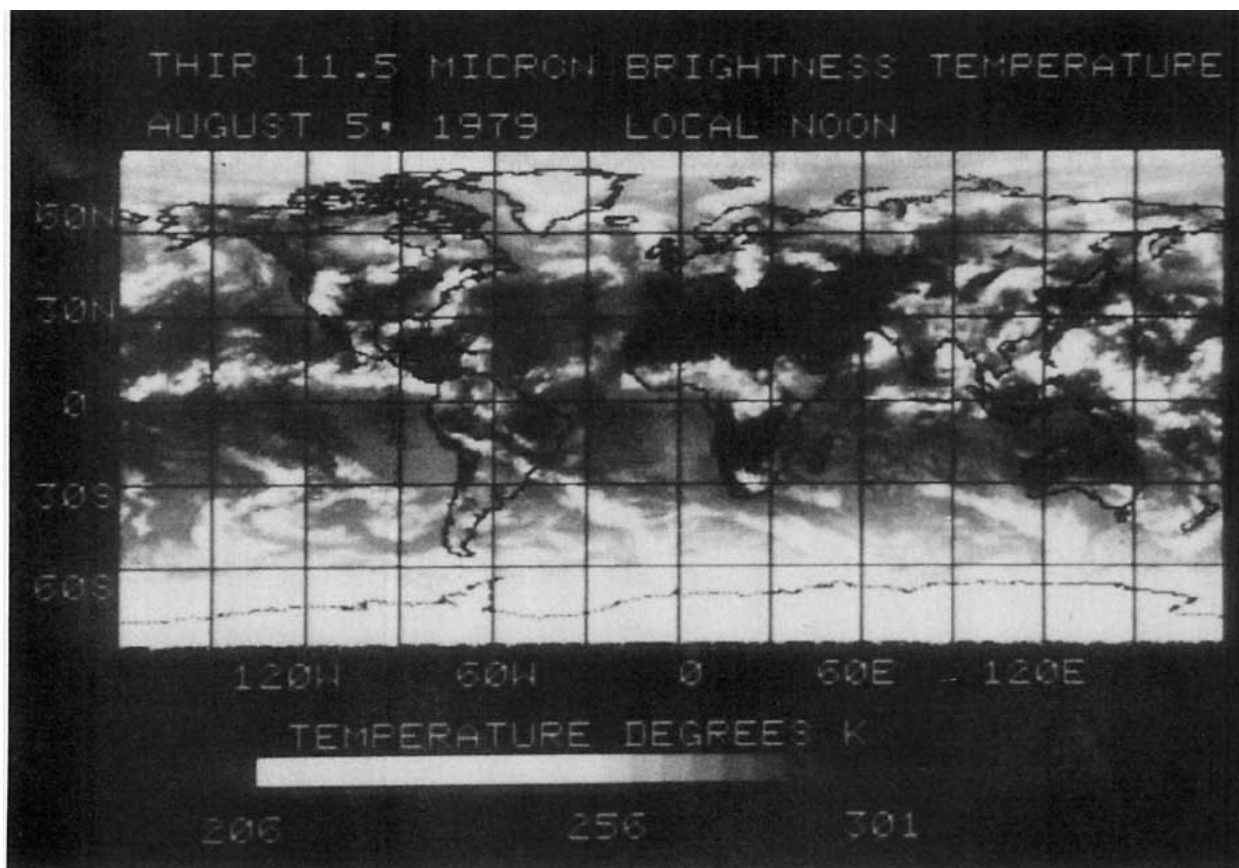


FIG. 1. Global map of the THIR 11.5 μm equivalent blackbody temperatures for 5 August 1979 at local noon. All brightness temperatures less than 256 K are depicted as white in the map.

of the incoming solar irradiance at these wavelengths, which are used to compute directional albedos from the backscattered radiances.

For each TOMS FOV, the surface reflectivity at 0.360 and 0.380 μm is estimated from the measured "scene" albedo by interpolation in a look-up table of directional "scene" albedos precomputed using a radiative transfer code (Dave 1964) for a variety of viewing and illumination geometries and pressures of the reflecting surface. The pressure of the reflecting surface is computed from an area weighted average of the terrain surface pressure and a climatological cloud amount and cloud top pressure (Fleig et al. 1982). The resulting estimate of reflectivity at these two wavelengths are then averaged. This averaged 0.37 μm UV surface reflectivity has a precision of 0.3%, and long-term stability better than 2.0% over the entire six-year dataset, as inferred from the measurements of diffuser plate stability by the Solar Backscatter Ultraviolet (SBUV) Instrument (Cebula et al. 1988). The cross track scanning of the instrument results in complete daily coverage of the globe, with the FOV varying from 50×50 km at nadir to 150×200 km in the extreme

off nadir position. In-flight calibration of the TOMS instrument includes electronics calibration to check the gain stability of the signal processing and wavelength calibration to detect wavelength shifts in the monochrometer.

The global distribution of the TOMS 0.37 μm reflectivity for 5 August 1979, is shown in Fig. 2. This is the same day as the map of the THIR 11.5 μm equivalent blackbody temperature in Fig. 1. It is evident from these images that cloud information can be derived from these two datasets. The two maps show that the major global cloud features such as the intertropical convergence zone (ITCZ) and midlatitude cyclones are detected by both instruments. There are differences also in the radiances measured by the two instruments, which enhance the information that may be retrieved for various cloud types. For example, it is noted that the cloudy regions north of Indonesia and in the Bay of Bengal appear to be much larger in the IR than in the UV image, which indicates thin high-level clouds (cirrus). Also, regions of relatively low altitude clouds, such as off the west coasts of North America, South America, and South Africa, are detected more readily

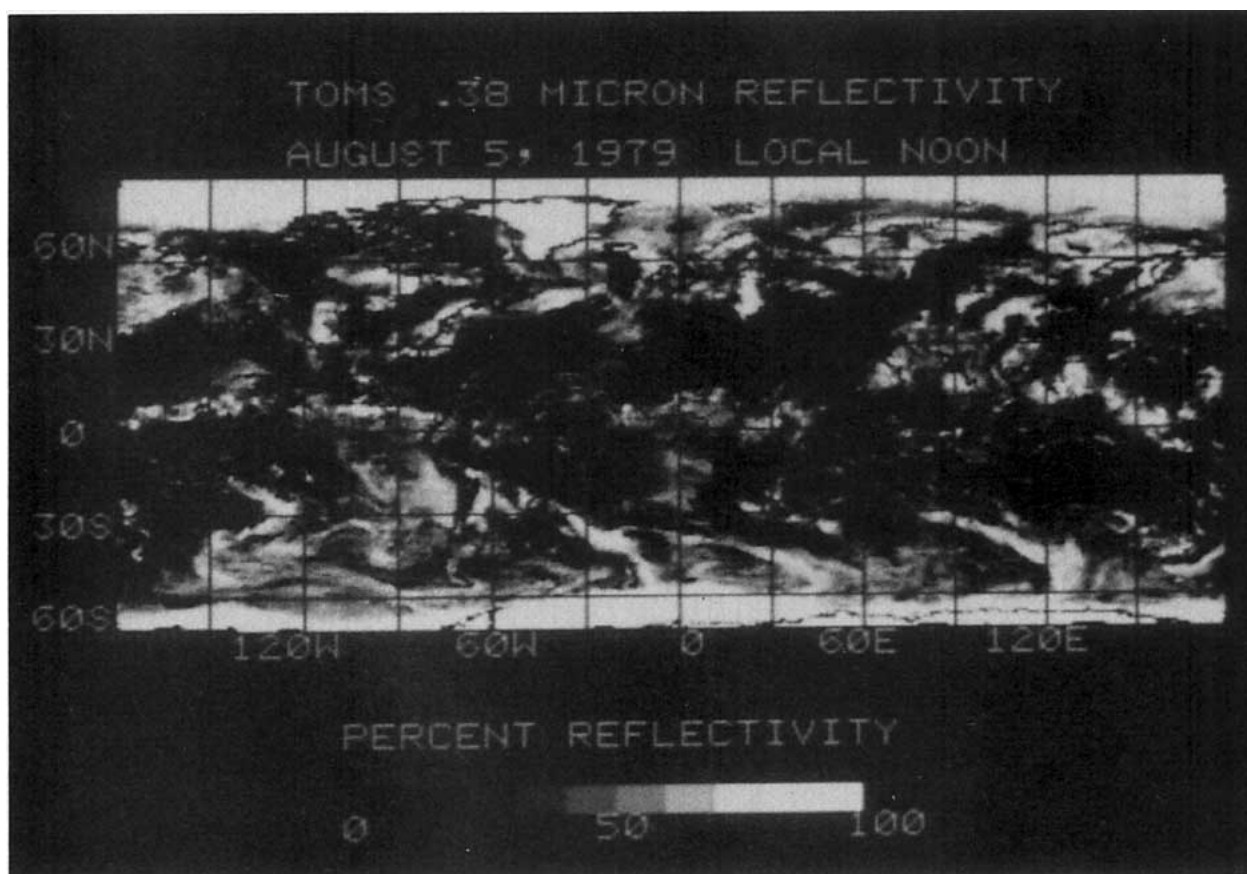


FIG. 2. Global map of the TOMS inferred UV reflectivity (%) at 370 nm for the same date and time as the THIR 11.5 μm brightness temperatures in Fig. 1.

from UV reflectivity measurements over the dark ocean surface than from the IR, where the thermal contrast with the sea surface is relatively small.

c. Air Force analysis

Three of the data fields used in the Air Force 3-D Cloud Nephanalysis (Fye 1978) have also been used in the Nimbus-7 cloud analysis: the Terrain Height Analysis, the Snow/Ice Analysis, and the Surface Temperature Analysis. All are archived at NOAA's National Climate Data Center. These global analyses use a 512×512 grid overlying a polar stereographic projection of each hemisphere, yielding a resolution of about 40 km at 60 degrees of latitude. The terrain height is reported at each grid point in tenths of meters. The snow/ice data were remapped onto a 1° latitude \times 1° longitude snow/no snow grid. The grid point closest to the location of each TOMS FOV is assumed to describe the snow/no snow conditions within the FOV. The snow analysis over land is updated at 00Z every day, and the ice analysis is updated weekly. In compiling its snow/ice analysis, the Air Force calls on inputs from hourly conventional surface reports, weekly Navy sea ice analyses, satellite radiometer observations, and climatology (Lucas et al. 1975). Beginning in January 1984, daily estimates of snow/no-snow were computed at each grid point by linear interpolation between monthly mean values. Prior to then, the daily analyses were used.

The surface temperature analysis over land is based on conventional shelter temperature reports from NMC and Air Weather Service Stations, which are received every three hours. Over water, the analysis uses sea surface temperature measurements reported by ships every six hours and by satellite remote sensing, twice daily. Initially, a five-layer atmospheric general circulation model is used to analyze the state of the atmosphere at a grid resolution of 320 km. This analysis is interpolated to a resolution of 160 km, and climatological lapse rates are used to extrapolate temperature from the gradient level (60 mb above terrain height) to the surface. Empirically derived diurnal temperature corrections are then applied to the surface temperature field. The most current shelter and sea surface temperature reports are then incorporated into the analysis using a modified Barnes technique. The global field is then interpolated to the final 40 km grid resolution. Finally, the most current conventional reports are again incorporated into the analysis. This procedure is repeated every three hours and the resulting analyses are archived on magnetic tape, beginning with 1 April 1979. The validation of these datasets is described in section four.

3. Cloud detection algorithms

In late 1982, NASA's Nimbus-7 Project Office formed a Cloud Data Processing Team (CDPT) to im-

plement an accurate method for cloud detection using THIR and TOMS observations. It was formed with the objective of improving the accuracy of cloud amount estimates derived from an earlier algorithm that used THIR 11.5 μm window radiance and climatological surface and atmospheric temperature data (Stowe 1984). The improved method uses two independent estimates of total cloud amount: 1) the "infrared (IR) algorithm", a threshold technique based on the 11.5 μm radiance measurements of THIR, but using concurrent surface temperature analyses in place of climatology, and accounting for uncertainties in specifying the cloud/no-cloud threshold; and 2) the "ultraviolet (UV) algorithm", a linear interpolation method based on the 0.37 μm surface reflectivity measured by TOMS. These two cloud-amount estimates are combined by a "bispectral algorithm" into one value of cloud amount. Each of these algorithms will be discussed in the following subsections.

a. Infrared algorithm

Each THIR 11.5 μm radiance observation (pixel) is classified as being either clear, low, middle, or high altitude cloud depending on its magnitude relative to precomputed radiance thresholds. Figure 3 is an illustration of the threshold setting procedure. Each of the items shown is determined as follows for each of the 18 630 approximately equal area ERB Subtarget areas (STA), each about $(165 \text{ km})^2$, completely covering the Earth's surface:

1) SURFACE TEMPERATURE FROM AIR FORCE

The temperature at the Earth's surface at a time within one-half hour of a Nimbus-7 overpass is determined from time interpolation of the STA average surface temperature derived every three hours from the Air Force Surface Temperature analysis archival dataset.

2) ADJUSTMENT FOR ATMOSPHERIC ATTENUATION

The Air Force surface temperature, T_{AF} is converted to an equivalent blackbody radiative temperature T^* (i.e., the expected clear-sky temperature that should be detected by the 11.5 μm channel of THIR when no clouds are within its FOV) by subtracting an empirical atmospheric water vapor attenuation adjustment, ΔT , i.e., $T^* = T_{\text{AF}} - \Delta T$. This adjustment was derived from colocated and concurrent observations of sea surface temperature and 11.5 μm radiance data from a NOAA scanning radiometer (Brower et al. 1976). The tabulated relationship between ΔT , satellite zenith angle, θ , and T_{AF} , has been represented by a second order polynomial fit of the form,

$$\Delta T = C_0 + C_1 T_{\text{AF}} + C_2 T_{\text{AF}}^2 + C_3 \theta + C_4 \theta^2 \quad (1)$$

where $C_0 = 70.3188$, $C_1 = -0.5516$, $C_2 = 0.0011$, C_3

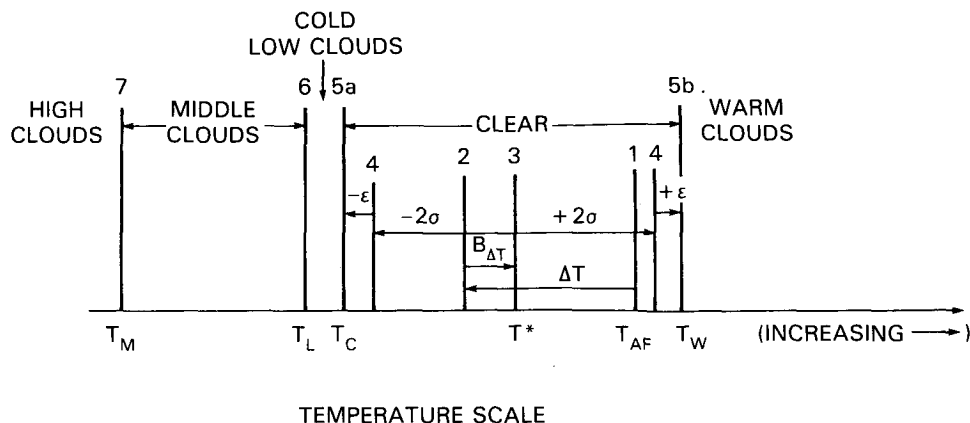


FIG. 3. The thresholds for the improved Nimbus-7 infrared cloud algorithm (BCLE). The following numbered items correspond to the numbers in the figure: 1) surface temperature from Air Force analysis, T_{AF} ; 2) adjustment for atmospheric attenuation (2° – 8° C), ΔT ; 3) bias in attenuation adjustment (2° C), $B_{\Delta T}$ and T^* , expected clear-sky temperature; 4) twice the standard deviation of expected clear-sky temperature due to humidity and horizontal temperature gradients, $\pm 2\sigma$ ($\geq 4^{\circ}$ C); 5) adjustment for partially filled fields of view (2° C), $\pm \epsilon$. [(a) cold cloud/no-cloud threshold, T_C , and (b) warm cloud/no-cloud threshold when climatological inversion present and when $T_{AF} < 280$ K, T_W .]; 6) low/mid cloud threshold, T_L ; and 7) mid/high cloud threshold, T_M .

$= 0.0037$, $C_4 = 0.0004$, with ΔT and T_{AF} in degrees Kelvin and θ in degrees.

This adjustment is not directly a function of water vapor amount, but in as much as water vapor content normally depends on surface temperature, this empirical relationship contains that dependence. The validity of this treatment of water vapor attenuation is discussed in Section 4a(2).

3) BIAS IN ATTENUATION ADJUSTMENT

The calculation of ΔT may contribute systematic errors in the estimate of T^* appropriate for THIR due to differences between the spectral response functions of THIR and the NOAA Scanning Radiometer or because of insufficient tropical ocean data or the lack of any land observations in the empirical dataset from Brower et al. Also, random errors may result from departures of the true attenuation adjustment from the empirical one because of natural variations in the relationship between humidity and surface temperature from the effective mean conditions represented in the empirical relationship (1). Theoretical and empirical studies were conducted to characterize the magnitudes of these errors. Results from these studies agreed that, for either land or ocean areas, the empirical formula overestimated ΔT by 2° C and had a standard deviation, $\sigma(\Delta T)$, of 2° C. Thus, it was concluded that the C_0 coefficient in Eq. (1) should be reduced by 2° C, i.e., $C_0 = 68.3188$.

4) UNCERTAINTIES IN ESTIMATING THE CLOUD/NO-CLOUD THRESHOLD

In addition to the random error in the computation of ΔT , discussed above, random uncertainty in the de-

termination of T^* also results from horizontal variations in the surface temperature field within a STA as analyzed by the Air Force. The standard deviation of the Air Force surface temperatures, $\sigma(T_{AF})$ at local noon and midnight, the time of the Nimbus-7 overpass, is computed for each STA. It ranges between values near zero for open ocean areas, to values exceeding 20° C for coastal or mountainous STAs, though the nominal value over land is 1° to 2° C. Also, the measurement of the $11.5 \mu\text{m}$ radiance contains random error. However, the standard deviation of these radiances for a uniform scene has been observed to be less than one digital count (about 0.5° C, cf. Hwang 1982), small by comparison with the other errors and is considered negligible. Thus, the standard deviation of the combined random errors, σ , due to atmospheric attenuation and horizontal temperature variations, is computed from the expression,

$$\sigma^2 = \sigma(\Delta T)^2 + \sigma(T_{AF})^2 \quad (2)$$

assuming that these errors are independent and uncorrelated. If we further assume that these random errors are Gaussian in distribution, with a zero mean value, and desire that the estimated radiative temperatures for a clear scene span a range that contains the observed clear radiative temperature with a probability of 95%, $\pm 2\sigma$, we must define two cloud/no-cloud thresholds, a cold threshold T_C and a warm threshold, T_W given by the formula,

$$\left. \begin{aligned} T_C &= T^* - 2\sigma \\ T_W &= T^* + 2\sigma \end{aligned} \right\} \quad (3)$$

5) ADJUSTMENT FOR PARTIALLY FILLED FOV

All threshold techniques suffer from another source of systematic error. When cloud elements are smaller than the FOV of the radiometer, and, if for example, the threshold is chosen to represent completely clear FOVs, then these partly cloudy radiances, which will typically be lower than the clear threshold, will be classified as totally cloud covered. This causes cloud amount to be systematically overestimated (Coakley and Bretherton 1982). We have computed an adjustment, ϵ , to correct for this error in the cloud/no-cloud threshold. It was estimated from histogram analyses of $11.5 \mu\text{m}$ THIR radiances over oceans that were either perfectly clear or that exhibited one clear and one cloudy mode. The clear histograms were analyzed to determine the mean displacement of the lowest temperature of the distribution (i.e., the ideal cloud/no-cloud threshold) from the modal clear scene temperature. The mean value of this displacement was 2.5°C . The partly cloudy histograms were analyzed in the same way, except that the ideal threshold temperature was chosen to give a cloud amount in agreement with an analyst's estimate based on GOES visible and infrared images. In this analysis, the mean displacement of the ideal threshold from the modal clear scene temperature was 4.5°C . The difference between these two mean displacements of the ideal cloud/no-cloud threshold and the clear modal temperature is assumed to be the mean value of the partially filled FOV adjustment, i.e., $\epsilon = 2^\circ\text{C}$. In actuality, this adjustment will vary with cloud temperature and amount, but as proper treatment of this would require a more complicated and costly iterative approach to the data processing, a mean correction for the partially filled field of view bias has been adopted.

Thus, the final value of the radiative temperatures for the cold threshold, T_C , and warm threshold, T_W , is computed from the expressions,

$$\begin{aligned} T_C &= T^* - 2\sigma - \epsilon \\ T_W &= T^* + 2\sigma + \epsilon \end{aligned} \quad (4)$$

Thus, over oceans, the cloud/no cloud thresholds are about 6°C away from the expected clear sky radiative temperature, a value consistent with the results of Coakley (1987), where a six to seven degree threshold was found to give good agreement with cloud amounts derived by the spatial coherence method. Over land, these thresholds are more variable, but are typically about 7° to 8°C away from T^* .

When a climatological inversion is present in a STA and the Air Force surface temperature is less than 280 K, any pixel with a radiative temperature greater than T_W is assumed to come from a cloud near the inversion and is classified as warm cloud and included in the LOW CLOUD category. Pixels with temperatures lower than T_C are classified as either middle or high

cloud, depending on whether the low/middle or middle/high threshold values, to be described next, are greater than T_C . This is an aspect unique to this IR algorithm, permitting clouds which are warmer than the Earth's surface (so-called "black clouds") to sometimes be detected. The surface temperature limit was imposed to eliminate clear desert regions, where the skin temperature frequently exceeds T_W , from being interpreted as covered by "warm clouds," and yet allow their detection in areas where they have been most frequently found to occur in other cloud analyses, such as the Air Force 3-D Nephanalysis. These areas are typically found in the winter hemispheres at high latitudes, where the surface air temperatures are usually well below 280 K, while the desert regions typically have air temperatures well above 280 K. For most of the Earth's surface, "warm-cloud" conditions do not exist, and the only cloud/no cloud threshold used in the IR algorithm is T_C (cf. section 4d for an example of warm cloud coverage).

6) THE LOW/MID CLOUD THRESHOLD

The altitude separating low from middle level clouds is assumed to be 2 km above mean sea level, consistent with the definition found in the International Cloud Atlas (WMO 1956). The temperature at that altitude, T_L , is computed for each STA from the formula

$$T_L = T_{AF} + (2 - Z_0)(dT/dZ)_L \quad (5)$$

where $(dT/dZ)_L$ is the climatological lapse rate between the surface and 2 km altitude for the appropriate month as computed from the NCAR monthly climatology (Jenne et al. 1974), and Z_0 is the altitude of the surface above mean sea level. In regions where the surface altitude is at 2 km or above, no low cloud bin is allowed.

The radiative temperature of the low/mid threshold, T_L^* , is computed by subtracting from T_L in (5) a fraction of the atmospheric attenuation adjustment, ΔT , used in computing the cloud/no-cloud threshold. That fraction was found to be $0.32 \times \Delta T$ from averaging numerous radiative transfer computations, in the $11.5 \mu\text{m}$ window, of the ratio of atmospheric attenuation of a blackbody at an altitude of 2 km to the attenuation of a blackbody at the surface. Also, it was assumed that the two sigma uncertainty in the attenuation table is scaled by the same factor, i.e., $0.32 \times 2\sigma(\Delta T) = 1.3$. Thus, the radiative temperature appropriate for the low/mid threshold is given by the expression,

$$T_L^* = T_L - 0.32\Delta T - 1.3 \quad (6)$$

7) THE MID/HIGH CLOUD THRESHOLD

The altitude of the mid/high cloud threshold poleward of 30 degrees latitude is assumed to vary according to the following equation,

$$Z_M = 7 - 1.5\{1 - \cos[3(|\text{LAT}| - 30)]\}. \quad (7)$$

Equatorward of 30 degrees latitude, $Z_M = 7$ km. This definition is consistent with the International Cloud Atlas, and is representative of the gradual change in tropospheric thickness with latitude.

The temperature at that altitude, T_M , is computed for each STA by

$$T_M = T_L + (Z_M - 2)(dT/dZ)_M \quad (8)$$

where $(dT/dZ)_M$ is the climatological lapse rate between 2 km and a reference altitude Z_r , where $Z_r = 7$ km for latitudes between 0 and 30 degrees, $Z_r = 6$ km for latitudes between 30 and 60 degrees, and $Z_r = 4$ km for latitudes greater than 60 degrees.

The atmospheric attenuation in the $11.5 \mu\text{m}$ channel for blackbody surfaces above the mid/high threshold is assumed to be negligible, so,

$$T_M^* = T_M. \quad (9)$$

The nominal subtarget area population of THIR samples varies from approximately 600 pixels at nadir to 100 at the extreme off-nadir. When only spatial sampling is considered, this implies that cloud amount can be estimated with a precision of better than 1%. Note: These temperatures, in addition to the other temperature thresholds, are converted to radiance units prior to pixel classification using a precomputed table of filtered radiance versus equivalent blackbody temperature, Hwang (1982).

b. Ultraviolet algorithm

The average surface reflectivity inferred by the TOMS instrument at $0.37 \mu\text{m}$ (cf. section 2b) is used to compute an independent estimate of total cloudiness for each STA. The average reflectivity from all TOMS FOV measurements located in each STA is used to determine total cloud amount for that STA. The UV reflectivity measured by TOMS for cloudless scenes has been investigated by using case studies with GOES images to determine cloudless areas and also by mapping the minimum reflectivity for a 3-month season over the entire earth (Eck et al. 1987). TOMS reflectivities are found to be very low and highly uniform for both land and water scenes, which are snow and cloud free. For example, clear scene ocean reflectivities are 6%–8%, typical Saharan desert reflectivity is also 6%–8%, and vegetated land areas have UV reflectivities that range from 2%–5%. This uniformity of land surface UV reflectance is an advantage over the visible reflectance which is highly variable, ranging from a few percent for vegetated surfaces to as high as 40% for deserts (Ashburn and Weldon 1956; Coulson and Reynolds 1971). Another advantage of UV surface reflectivity is that it is much less dependent on solar illumination angle and satellite viewing angle than is the visible. This is due to stronger Rayleigh scattering at $0.37 \mu\text{m}$, which diffuses much of the UV that reaches the surface, and upon reflection, scatters the UV again in passing

through the atmosphere before being sensed by the satellite.

Since STAs are fairly large in area ($165 \text{ km} \times 165 \text{ km}$), it is likely that many will be partially cloud covered. Provided that these STAs are sunlit, cloud amount is estimated from a linear relationship between UV reflectivity, averaged for all snow-free TOMS observations in an STA, and cloud amount. There has to be at least one TOMS observation that is determined to be snow-free. To illustrate the validity of this relationship, the TOMS reflectivity and its standard deviation are plotted in Fig. 4 as a function of IR total cloud amount for a one-week period from 2–8 December 1979, from 60°N to 60°S latitude. Even though the plotted relationship is nonlinear, it has been concluded that the line that is shown to vary between 8% and 50% in TOMS reflectivity as cloud amount varies between 0% and 100% is the correct relationship, for the following reasons: 1) the average reflectivity observed at 100% cloud amount is seen to exceed the value chosen for the linear relationship. This higher value of reflectivity was disregarded for the following reason. Figure 5, based on an analysis of 205 days of ocean STA observations from 1979 and 1980, shows that as IR cloud amount varies from 0% to 100%, the proportion of clouds at low, middle and high altitudes also varies. At small cloud amounts, low altitude clouds predominate, but as cloud amount increases, middle cloud gradually predominates. At 95%–100%, middle and high altitude clouds predominate. It is thus hypothesized that the elevated reflectivity of TOMS at 100% cloud cover results from the increased proportion of high altitude cloud, these potentially being geometrically thicker and therefore brighter than other clouds. Since the UV cloud amount estimate is used as a correction for the IR algorithm when the latter indicates either low clouds or no clouds are present (see section 3c), it was decided to use 50% for the upper limit of reflectivity. This value is more likely to be representative of low altitude (less thick) clouds and is more consistent with the observed change in reflectivity with cloud amount as the amount increases from 50% to 100%; and 2) the linear relationship was chosen to be below the plotted points when cloud amount is small since, as is discussed in section 4, the IR algorithm tends to systematically underestimate cloud amount when the cloud is low in altitude, which is the predominant cloud type when cloud amount is small, as shown in Fig. 5. A reflectivity of 8% to represent 0% cloud amount was selected from results of analyses for clear ocean surfaces, the predominant surface type on the earth. It is noted that there are some regions on the Earth where the cloudless scene UV reflectivity inferred by TOMS always exceeds 8%. These few STAs will always be interpreted as being covered by small amounts of cloud. These STAs are located in the sandy desert regions of the Libyan desert and parts of the Saudi Arabian peninsula, where TOMS reflectivity ranges from 9%–12%.

**TOMS REFLECTIVITY AS A FUNCTION OF
INFRARED CLOUD AMOUNT
DECEMBER 2 - 8, 1979**

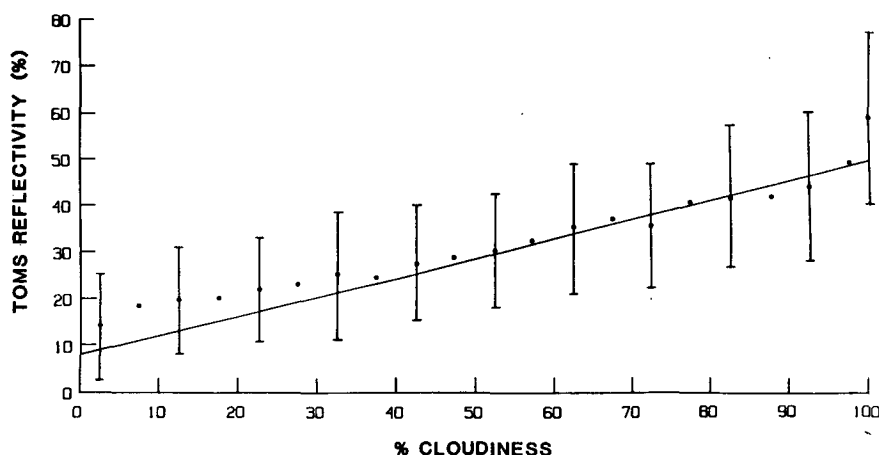


FIG. 4. TOMS inferred reflectivity as a function of the infrared algorithm total cloud amount for the region 60°S to 60°N for 2–8 December 1979. The bars denote plus and minus one standard deviation. The heavy line is the UV linear algorithm chosen to relate an 8%–50% reflectivity range with a 0%–100% cloud amount range.

c. Bispectral algorithm

The bispectral algorithm has been designed with the objective of deriving the most accurate estimate of total cloud amount from the two independent UV and IR estimates available for each STA. The infrared estimate is more accurate than the UV estimate for middle and

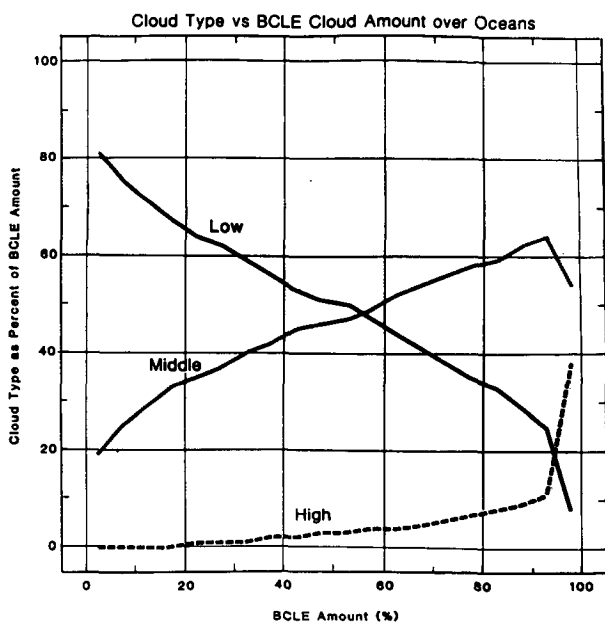


FIG. 5. The percentage of IR algorithm (BCLE) cloud amount, by type of cloud (low, middle, high), versus the total cloud amount of the IR algorithm, for 205 days of 1979 and 1980. Low altitude cloud dominates for small total cloud amounts, while mid and high altitude cloud is dominant for large total cloud amounts.

high altitude clouds, since the IR has little difficulty in sensing these clouds due to the large thermal contrast with the surface and because the UV reflectivity is highly variable for these kinds of clouds, being sensitive to cloud thickness variations as well as to changes in cloud amount. However, when low clouds or no clouds are present, the UV algorithm is more accurate than the IR since the infrared contrast between the cloud and the underlying surface is small, comparable with the uncertainty in determining the cloud/no-cloud threshold. (This logic is quantitatively demonstrated in section 4b.) Low cloud is relatively easy for the UV to detect accurately because of the large contrast in reflectance between the snow-free or ice-free surface and the low cloud. Also, UV reflectance of low clouds is more closely related to cloud amount and less affected by cloud thickness, since low clouds are confined to the lowest levels of the atmosphere and, therefore, cannot vary as greatly as middle or high altitude clouds.

Conceptually, then, the bispectral algorithm should result in total cloud amounts close to the infrared estimate when the IR algorithm indicates a large amount of middle and high altitude cloud, but should approach the UV estimate when IR low cloud and clear amount are large. A mathematical form for this bispectral algorithm is given by

$$NCLE = BCLE * (1 - W) + TOMS * W \quad (10)$$

where

$$W = W_1 * W_2$$

$$W_1 = \cos(\theta)$$

$$W_2 = (\text{clear} + \text{low})/100.$$

NCLE and BCLE are acronyms for New and Basic Clouds for ERB, i.e., the bispectral and IR algorithm STA products, respectively; TOMS is used to represent the UV algorithm STA cloud estimate.

The total weight, W , is a composite of two weights, W_1 and W_2 . The factor W_1 reduces the influence of TOMS in the bispectral algorithm as satellite zenith angle increases because of the larger FOV of TOMS compared to THIR. The TOMS FOV eventually becomes larger than the average size of an STA as satellite zenith angle (θ) increases, while the THIR FOV remains much smaller than an STA, thus making the TOMS estimate less reliable than the BCLE estimate. The reduction in the number of TOMS FOVs located in a STA is approximated by $\cos(\theta)$, which is used to compute W_1 . The value of W_1 typically ranges between 0.5 and 1.0. The weight W_2 is simply the fraction of the STA that is determined by the IR algorithm to be clear and/or covered by low cloud. For the same satellite zenith angle, the larger the fraction of the STA that is clear and/or covered by low cloud, the closer the bispectral algorithm cloud amount will be to the TOMS estimate. The smaller that fraction, the closer the bispectral algorithm cloud amount will be to the BCLE estimate.

When the TOMS observes less cloud than BCLE, the BCLE low, then mid and then high cloud amounts, in that order, are decreased to agree with the bispectral total cloud amount, NCLE. If no THIR pixels were classified as clear, then the clear temperature corresponding to the NCLE value of clear created by the bispectral algorithm is computed by adding (subtracting) 6°C, the minimum value of the uncertainty terms in Eq. (4), to the cold (warm) cloud/no-cloud threshold temperature. The operation in parentheses is used when the warm cloud criteria are satisfied. When TOMS observes more cloud than BCLE, the BCLE low cloud amount is increased so that it, when added to the BCLE estimates of mid and high cloud amount, agrees with the NCLE total cloud amount. If no low cloud was observed by BCLE, the low cloud temperature is assumed to be at the appropriate cloud/no-cloud threshold temperature, depending again on whether the warm cloud criteria are satisfied. The NCLE middle and high cloud temperatures are the same as the BCLE-derived values.

At night and also when snow completely covers a STA, no adjustments are made to any of the IR algorithm estimates, i.e., the BCLE results are used.

Once the bispectral clear, low, mid, and high amounts have been established, the TOMS reflectivity together with the IR algorithm cloud amounts can also be used to identify the presence of cirrus and deep convective clouds. The principle behind the cirrus identification method is as follows: if the IR algorithm determines that there is a substantial amount of cold (high altitude) cloud and the TOMS reflectivity is relatively low, then the cloud is identified as cirrus. Only cirrus

without underlying cloud can be detected with this technique since low UV reflectivity is the main criteria used to distinguish cirrus from other cloud types. The identification of deep convective cloud follows this principle: if the IR algorithm detects a substantial amount of cold cloud and the TOMS reflectivity is relatively high, then the cloud is identified as deep convective.

Based on analysis of GOES visible and infrared images for regions with cirrus clouds, a linear relationship between reflectance and amount in an STA was identified, where reflectivity varies between 8% and 35% as cirrus cloud amount varies between 0% and 100%. If this TOMS cirrus cloud amount estimate is less than or equal to the IR algorithm (BCLE) total cloud amount estimate in the STA, and if the middle cloud radiance at 11.5 μm is lower than the average of the low/mid and mid/high cloud boundary radiances, then the bispectral algorithm (NCLE) middle and high cloud amounts are combined to yield the estimate of cirrus cloud amount. If the middle cloud radiance is higher than the average boundary radiance, only high cloud amount is used as the cirrus amount estimate. Clouds that are warmer (lower altitude) than this boundary are excluded to avoid misclassifying fairly thin or scattered low clouds, or regions of high water vapor amount as cirrus cloud.

In the deep convective algorithm, an estimate of the amount of deep convective cloud is made from the TOMS reflectivity using the linear relationship, 8%–75% variation in reflectivity corresponds to 0%–100% variation in cloud amount. This reflectivity/cloud amount relationship for deep convective clouds was chosen as a result of a statistical analysis of reflectivity for TOMS FOVs which were 100% filled with high cloud as detected by the IR algorithm. The mean reflectivity of the high cloud for a one-week period, 24–30 June 1979, for 60°N to 60°S was 76%. Then, if the TOMS deep convective estimate is greater than or equal to the IR algorithm total cloud amount, the NCLE high cloud amount is chosen as the deep convective cloud amount.

Neither of these two special algorithms changes the NCLE estimates of low, middle, or high cloud amount. They simply are used to estimate the amount of cirrus and deep convective cloud present.

d. Archived tape products

The STA results of the BCLE, TOMS and NCLE algorithms, described in sections 3a–3c, and ancillary data, as described in Table 2, are stored on 1600 bpi magnetic tape and archived weekly. This is referred to as the NCLE dataset.

Each month of NCLE data is further processed into ERB target area (TA) averages (500 km)², referred to as the Cloud–Matrix (CMATRIX) dataset. Both daily and monthly averages are given. Each 6250 bpi tape contains one data year of cloud amount and radiance

TABLE 2. Archival products list.

<i>New cloud-ERB tape (NCLE)</i>	
Source	THIR, AFST, STAGs, ILT, BCLE and TOMS AFST—Air Force surface temperature STAGs—Climatological temperature data ILT—Image location data
Coverage	Orbit-by-orbit observations
Frequency	Twice a day
Parameters	40/STA; includes low, middle, and high cloud amount and clear amount (bispectral and IR); mean and RMS radiances at 11.5 μm and 6.7 μm for the above amounts; min and max observed radiance at 11.5 μm ; mean TOMS reflectance and cloud amount; mean amount and altitude of land; cirrus and deep convective amount; geometry, time, IR thresholds, number of THIR pixels and mean AFST.
Resolution	Subtarget area ($\sim 165 \text{ km}^2$)
Number of tapes	One 1600 bpi tape per week
<i>Cloud matrix tape (CMATRIX)</i>	
Source	NCLE
Coverage	Uses most nadir observations for overlapping orbits.
Frequency	Twice a day, daily and monthly average
Parameters	119 monthly and 75 daily for each TA; includes bispectral low, middle, high cloud and clear amounts and 11.5 μm radiances; total cloud amount and 11.5 μm radiance (bispectral and IR); geometry, time, and TOMS reflectivity; spatial RMS (daily) and temporal RMS (monthly) of all the above quantities; cirrus and deep convective amount; snow cover; IR thresholds, space and time sampling statistics; land amount; mean AFST and maximum 11.5 μm radiance; zonal, hemispheric and global statistics.
Resolution	Target area (TA) ($\sim 500 \text{ km}^2$) by averaging data for nine STAs (missing if more than six STAs/TA missing); zonal (missing if more than 50% of TAs/zone missing); hemispheric (missing if more than 25% of zonal area missing); global (missing if either hemisphere missing).
Number of tapes	One 6250 bpi tape per year

statistics and other relevant parameters as outlined in Table 2.¹

Note: The original form of the bispectral algorithm and the UV algorithm, which were used to process five years of NCLE and CMATRIX products during the period between June 1984 and June 1986, was found to cause a small (2%–4%) artificial increase in the frequency of occurrence of cloud amount in the range of 60% to 65% and to overestimate global and hemispheric cloud amount by about 2% relative to the final algorithm. However, the spatial and temporal character-

istics of global cloud cover were very similar to those resulting from the final algorithms reported in this paper. Therefore, results of studies using cloud products generated from the original algorithms (e.g., Stowe et al. 1986; Slingo 1987) should be insignificantly different if redone using the final algorithm results.

4. Validation

Validation of the Nimbus-7 cloud algorithms has been performed by: 1) analyzing the auxiliary data used in interpreting the satellite radiance data; 2) computing the sensitivity and expected errors in total cloud amount due to uncertainties in algorithm parameters; 3) statistically comparing Nimbus-7 cloud amount estimates with estimates from an analyst for quantitative validation; 4) comparing images constructed from Nimbus-7 cloud estimates with simultaneous but independent satellite cloud images; and 5) interpreting histograms and other displays of the data for qualitative validation. Each will be discussed separately in this section.

It will be shown that: (i) the Air Force surface temperature field, with the exceptions of Antarctica, probably Greenland and, prior to mid-July, 1979, Southern Hemisphere land, are suitable for use in the IR cloud algorithm; (ii) even though the Air Force surface temperature field is based on shelter temperature over land, where the skin temperature can exceed it by as much as 40°C, this field is still useful for cloud estimation with the Nimbus-7 IR cloud algorithm; (iii) the Air Force snow/ice analysis is adequate for identifying surfaces where the TOMS reflectance algorithm cannot be used; (iv) the computed errors in total cloud amount from the sensitivity analysis are in reasonable agreement with the errors inferred from a statistical comparison with an analyst's cloud estimates, the latter indicating that the satellite estimates have systematic errors less than 10% and random errors ranging from 7% to 16%, relative to the analyst; (v) cloud amounts over humid tropical regions tend to be overestimated with the Nimbus-7 algorithms, day or night, and marine stratocumulus clouds tend to be underestimated at night, when correction of the IR algorithm result by comparison with the TOMS reflectance is not possible; (vi) cirrus clouds are detected bispectrally when sufficiently thick to be classified as upper middle and high altitude clouds by the IR and when isolated from bright low level clouds or surface snow cover; (vii) the location of deep convective clouds from bispectral analysis is well correlated with locations on satellite imagery; (viii) "warm" clouds, clouds whose temperature is greater than the surface air temperature, are detected in regions where they frequently occur; and (ix) the total cloud amounts are weakly dependent on viewing angle, and frequency of occurrence of total cloud amount is a smoothly varying "U"-shaped function of cloud amount.

¹ These data may be obtained from the National Space Science Data Center, NASA/Goddard Space Flight Center, Greenbelt, MD 20771, 301/286-7134.

a. Validation of auxiliary data

1) AIR FORCE SURFACE TEMPERATURE ANALYSIS

The quality of the Air Force surface temperature analysis has been investigated by comparison with surface reports at 00Z and 12Z for a summer and a winter day in the Northern Hemisphere over ocean and land regions approximately $(250 \text{ km})^2$ in area. The results indicate that the Air Force analysis is typically within one degree of the surface station reports. The largest mean difference of -1.4°C (Air Force minus surface) occurred at 00Z on 11 June 1979 in Central Asia. This same area correctly exhibited the largest standard deviations, which result from the more greatly varying temperatures in the Air Force analysis, caused by variations in the height of the terrain. These large variations are not evident in the surface station reports, which are typically located in lower altitude areas.

There were no surface reports readily available for comparison with the Air Force analyses in the Southern Hemisphere, but a limited number of radiosonde reports were obtained. The conclusion from these limited comparisons was that the Air Force analyzed temperatures agreed with the radiosonde surface air temperatures to better than five degrees Celsius on both dates at both times, except for the high-altitude regions of Antarctica. The Air Force analysis may be overestimating the surface temperature in the interior of Antarctica by between 40° and 60°C . (There is evidence that the same may be true of Greenland in the Northern Hemisphere.) Antarctica is the site of the only anomaly that appears to be persistent throughout the archival record from April, 1979. As a result, the Nimbus-7 cloud analysis scheme uses monthly mean climatological surface temperatures (Jenne et al. 1974) for all latitudes south of 63°S .

One other anomaly, but of limited duration, is worthy of mention. For some unknown reason, the diurnal variation of temperature in the Air Force analyses for land areas in the Southern Hemisphere was out of phase, such that the maximum daily temperatures occurred near 2100 local time (LT) and the minimum at 0900 LT. The normal time for these temperature extremes is about 1400 and 0500 LT, respectively. This anomaly exists for about two and one-half months, beginning 1 April 1979.

2) ADJUSTMENT FOR ATMOSPHERIC ATTENUATION

In order to validate the Air Force surface temperature analysis and the adjustment for atmospheric attenuation, an analysis of the difference between the THIR $11.5 \mu\text{m}$ radiative temperature for cloudless scenes and the Air Force surface temperature corrected for atmospheric attenuation [T^* in section 3a(2)] was performed using a dataset with resolution of the TOMS FOV. Figures 6 and 7 are maps of the average of this temperature difference for the time period 17 June–25

August 1979, for local noon and local midnight, respectively. For local noon observations, cloudless cases were identified by using only those observations that had a TOMS reflectivity of 8% or less. The white areas in Fig. 6 are regions where, over the time period analyzed, the TOMS reflectivity exceeded 8% for all observations due to the presence of some cloud or, in the case of some desert regions, due to surface reflectances between 9%–12%. This figure shows that over the clear oceans, the computed value of T^* is within $\pm 1^\circ\text{C}$ of the measured THIR radiative temperature, except in the northern tropics, where the radiative temperature from THIR is typically 2° – 4°C lower. These greater differences in the tropics, centered on the ITCZ region, are due either to large amounts of water vapor in excess of those amounts represented by the atmospheric attenuation adjustments (3) or due to very thin cirrus clouds. Thus, over the extratropical oceans, the atmospheric attenuation adjustment applied to the Air Force surface temperature analysis does very well at estimating the THIR $11 \mu\text{m}$ clear radiative temperatures and, considering the uncertainties involved in the estimation of the cloud/no-cloud threshold [section 3a(5)], adequately in the tropics.

Over many land areas, however, we observe that the radiative temperatures measured by THIR are systematically higher than the Air Force surface temperature adjusted for atmospheric attenuation. This is because the Air Force analysis uses air (shelter) temperatures over land, whereas surface (skin) temperatures were used over oceans. The differences observed over land are primarily the result of differences in air and skin temperature.

It is noted, however, that variations in surface emissivity can also contribute to the measured variation in the effective radiative temperature. Griggs (1968) found surface emissivity in the Mojave Desert to vary from 0.90 to 0.94 for the 8–14 micron band, with sand dunes having the lowest emissivity. For vegetation, the 8–14 micron emissivity is generally greater than 0.95 except for dehydrated leaves where the emissivity may be as low as 0.90 (Smith 1983). These surface emissivity variations result in differences between the surface thermodynamic temperature and its radiative temperature. Thus, the result of the variation in surface emissivity is that for some surfaces, deserts especially, the difference between skin temperature inferred from THIR and air temperature is somewhat less than the actual thermodynamic skin-air temperature difference.

The color scale in Fig. 6 shows that most of the Earth's desert and arid land surfaces are at least 10°C and sometimes as much as 25°C hotter than the overlying air temperature for the ascending (local noon) portions of orbits. In this map, it is also evident that there is a close relationship between the magnitude of the surface-air temperature difference at noon and the amount of vegetation on a gross continental scale. For example, the rain forest regions of the Amazon Basin

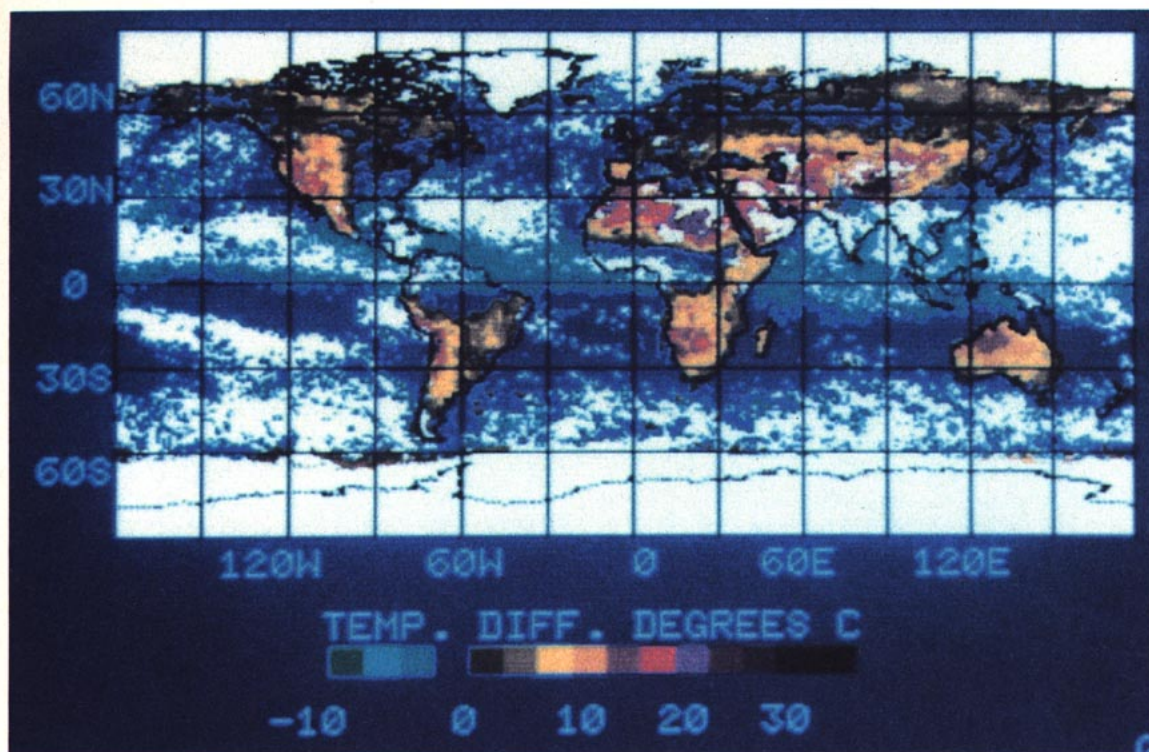


FIG. 6. Global map of difference between the THIR $11.5 \mu\text{m}$ radiation temperature for cloudless conditions and the Air Force surface temperature corrected for atmospheric attenuation, T^* . These temperature differences are the averages for all cloudless cases observed for the interval 17 June through 25 August 1979 at local noon. The criteria for selection of cloudless condition was a TOMS reflectivity of 8% or less. Areas never satisfying the criteria are white. Each color band in the scale represents a temperature interval of 3°C , except for dark blue which is -1° , 0° and $+1^\circ\text{C}$. For example, the bright red is for areas where skin temperature exceeds shelter temperature by $16^\circ\text{--}19^\circ\text{C}$.

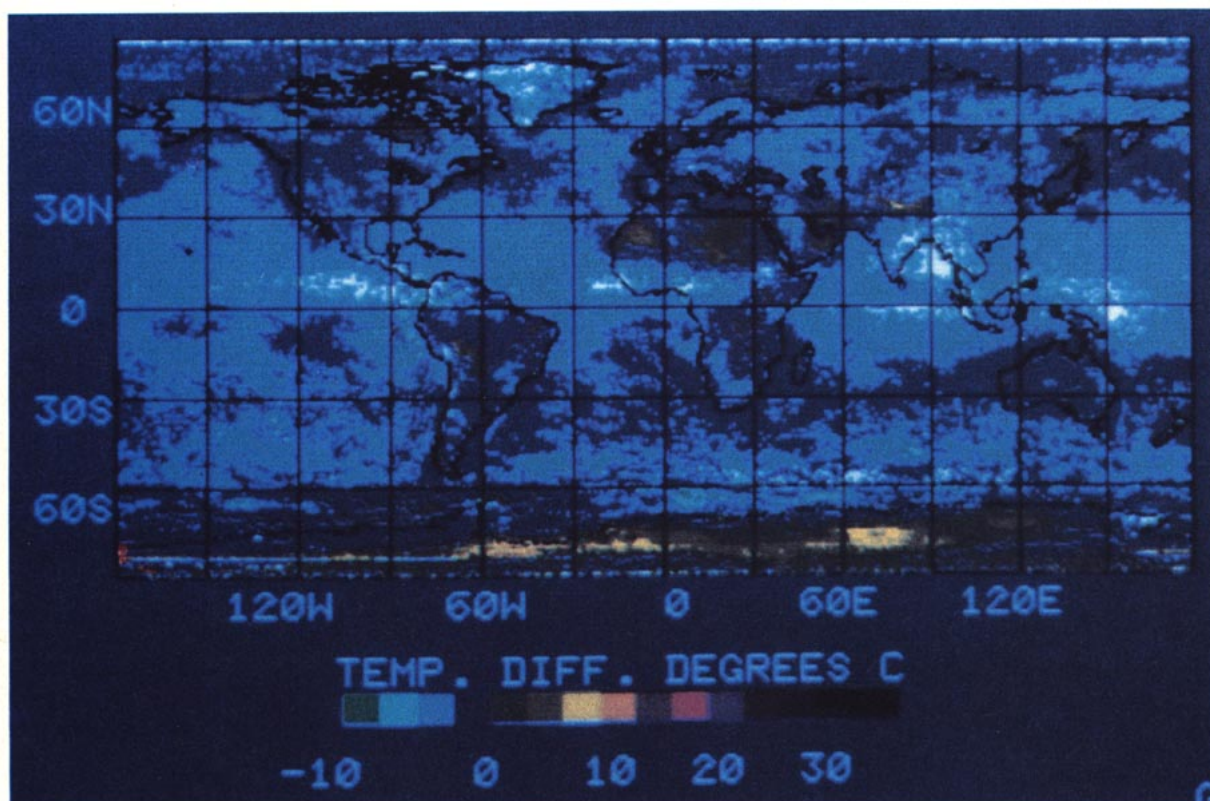


FIG. 7. Same as Fig. 6 but local midnight. The criteria used for selection of cloudless cases was that the infrared cloud algorithm (BCLE) detected 0% cloud.

and equatorial Africa have a surface-air temperature difference of $+1^{\circ}\text{C}$ and the midlatitude forests of eastern North America and Eurasia have a difference ranging from -1° to 4°C , which contrasts sharply with the large differences for arid regions. This general relationship between vegetation and the surface temperature regime is in agreement with the findings of Goward et al. (1985) from their study of a 20 km^2 site in Connecticut. They found from satellite observations that, as the measure of green vegetation amount increased, the magnitude of the effective radiance at $10.5\text{--}12.5\text{ }\mu\text{m}$ decreased, and concluded that the principal mechanism affecting the radiant surface temperature is the exchange of latent heat that occurs during transpiration. Nieuwenhuis et al. (1985) state that for vegetation that is well watered, most of the net radiation is used as latent heat for vaporization and that a decrease in latent heat flux results in a vegetation temperature increase and therefore an increase in sensible heat flux. Therefore, the large surface-air temperature differences over arid regions (Fig. 6) are probably largely due to the lack of moisture in the soil or lack of vegetation to provide for surface heat dissipation through evaporation or transpiration.

As discussed in Stowe (1984), the effect of this skin-shelter temperature difference in determining the cloud/no-cloud threshold over land surfaces is minimal because clouds tend to be colder than the shelter temperature. Also, with the improved NCLE algorithm, if partial cloud covered observations are warmer than the cloud/no-cloud threshold, the reflectance algorithm will correct the BCLE estimate for this problem. However, because thin cirrus can be difficult to detect in the UV (principle behind the bispectral detection of cirrus), its amount is likely to be underestimated when it occurs over hot desert regions.

The validity of the atmospheric attenuation adjustments over land is better seen in Fig. 7, where skin-shelter temperature differences are shown for the descending (local midnight) portions of orbits. No longer having the TOMS reflectance to judge clear sky conditions, we have used the IR only algorithm estimate of clear (0% cloud) to compute the difference between the THIR clear radiance and T^* . Over oceans, the skin-shelter temperature differences appear to be more negative by several degrees than during the daytime (cf. Fig. 6). This is so because the cloud/no-cloud threshold is designed to allow some pixels with partial cloud cover to be classified as clear. [cf. Sec. 3a(5)]. This would cause the observed decrease in the clear radiance of several degrees, on the average, from what would be observed when using TOMS reflectance to detect clear skies. The greater negative differences in the northern tropics in Fig. 6, are also evident in the nighttime data. Over land, the difference between skin and shelter is less than plus or minus 4°C , except for parts of the desert regions where, interestingly, the skin temperature is still as much as 7°C larger than the shel-

ter temperature near local midnight. Smith (1984) has shown from field observations that the skin temperature can indeed exceed the shelter temperature at local midnight in parts of the Saudi Arabian, Saharan, and Gobi deserts.

It is interesting that the climatological surface temperatures used for Antarctica cause the estimated clear radiative temperature (shelter) to be systematically lower than the observed (skin) value by up to 7°C , as seen in Fig. 7. This difference would cause cloud amount to be systematically underestimated, except when climatological inversions are present, in which case warm low cloud would be overestimated. Because of the high surface reflectance in the UV and the nearly isothermal lapse rate conditions, with THIR and TOMS data cloud estimates over polar snow or ice covered areas are uncertain—independent of the quality of the auxiliary information.

The daytime spatial distribution of skin-shelter temperature differences will vary with season of the year due to changes in the distribution of the amount of solar radiation available for heating the surface. However, the magnitude of this difference, and hence the effect on the IR cloud algorithm, should not be seasonally different.

It is thus concluded from results presented in sections 4a(1) and (2) that the Air Force surface temperature analysis, adjusted by the empirically derived, bias-corrected, attenuation table, can be used to estimate the clear-sky radiative temperature for the $11.5\text{ }\mu\text{m}$ channel of THIR over land and ocean areas with sufficient accuracy for computing the cloud/no-cloud threshold used in the IR algorithm. The sensitivity of the cloud amount algorithms to errors in the critical algorithm parameters is presented in section 4b.

3) SNOW/ICE COVER

Comparisons between the Air Force snow/ice analysis and NOAA/NMC and NESDIS snow analyses have been performed, showing qualitative agreement in the placement of the snow/no snow boundaries in the Northern Hemisphere. The Air Force has issued memoranda that confirm the validity of the snow/no snow boundary. However, there are some infrequently occurring anomalies in the analysis: 1) high elevation areas are snow covered year round, independent of whether or not they warm sufficiently to melt snow; 2) climatological snow cover is used to initialize the analyzed fields at the beginning of every month, causing discontinuities in snow cover between the end of one month and the beginning of the next; 3) Greenland is occasionally analyzed as being snow-free, e.g., from 6 to 31 July 1979; and 4) Antarctic sea ice occasionally disappears for a day or two and then reappears, e.g., 10 October 1979. Of these anomalies, the one involving Greenland is the only one that we have been able to fix. This was done by forcing Greenland STAs that do

not contain coastlines, to be snow covered all year round.

It is concluded that, due to the infrequent occurrence of these anomalies, the Air Force global snow/ice analysis is adequate for the purposes of identifying TOMS reflectances that may be snow contaminated and, therefore, not useful for estimating cloud amount.

b. Validation with sensitivity/error computations

The computation of error in total cloud amount has been done for each of the three algorithms: BCLE, TOMS and NCLE. The error formulas are derived from a theorem of differential calculus, stating that the total derivative of a function is equal to the sum of the partial derivatives of the function with respect to the function variables.

1) TOMS ALGORITHM ERROR COMPUTATIONS

The TOMS algorithm can be expressed as

$$N_T = a + bR. \quad (11)$$

The corresponding error formula has the form

$$dN_T = \frac{\partial N_T}{\partial a} da + \frac{\partial N_T}{\partial b} db + \frac{\partial N_T}{\partial R} dR \quad (12)$$

which is the total derivative of the TOMS total cloud amount, N_T , expressed as a function of the variables it depends upon; the TOMS reflectivity, R , a , the intercept and b , the slope of the line relating total cloud amount to reflectivity. To estimate the partial derivatives of cloud amount with respect to a , b and R , it is assumed that each variable is independent of the other two. Thus, from (11),

$$\frac{\partial N_T}{\partial a} = 1; \quad \frac{\partial N_T}{\partial b} = R; \quad \frac{\partial N_T}{\partial R} = b \quad (13)$$

The differentials in (12) are assigned the value of one standard deviation (SD) of the variable. Here SD is estimated by assuming that the extreme values of each variable defines the range of Gaussian distribution within which the variable has a 95% probability of occurrence, i.e., represents a range of four standard deviations. This is equivalent to having sampled each variable between 20 and 30 times if its range would have been estimated empirically (Ostle and Mensing 1975). The extreme values for slope and intercept are taken from the cirrus and deep convective algorithms (cf. Section 3c), and the extreme values of reflectance are taken from these same two algorithms for overcast conditions (OVC) and from Eck et al. (1987) for clear conditions (CLR). Thus,

$$da = |-29.6 - (-11.8)|/4 = \pm 4.4 (\% \text{ cloud})$$

$$db = |1.5 - 3.7|/4$$

$$= \pm 0.55 (\% \text{ cloud}/\% \text{ reflectivity})$$

$$dR(\text{CLR}) = |12\% - 4\%|/4 = \pm (2\% \text{ reflectivity})$$

$$dR(\text{OVC}) = |75\% - 35\%|/4 = \pm (10\% \text{ reflectivity}).$$

(14)

As an upper limit of the uncertainty in the derived cloud amount from the TOMS "total cloud" algorithm, we have let all the terms on the rhs of (12) be of the same sign. Thus, for clear conditions, where R is 8%, and for overcast conditions, where R is 50% in the TOMS total cloud algorithm, and substituting the terms from (13) and (14) into (12), the maximum estimate of the error is

$$dN_T(\text{CLR}) = \pm 13.6\%$$

$$dN_T(\text{OVC}) = \pm 55.7\%. \quad (15)$$

A more conservative estimate of the error in the TOMS algorithm is to assume that each error source on the rhs of (12) is statistically independent, i.e., the error terms combine as the square root of the sum of squares of the terms on the rhs of (12) (Beers 1958), giving

$$\left. \begin{aligned} dN_T(\text{CLR}) &= \pm 7.9\% \\ dN_T(\text{OVC}) &= \pm 36.6\% \end{aligned} \right\} \quad (16)$$

These results indicate that the uncertainty in the TOMS estimate of cloudiness is least for small amounts of cloud and greatest for large amounts of cloud. It was because of this characteristic of the TOMS algorithm that the particular form of the merge algorithm (10) was chosen, where more weight is given to the TOMS estimate when cloud amount is small and least when cloud amount is large, as discussed in section 3c.

2) BCLE ALGORITHM ERROR COMPUTATIONS

The uncertainty in the estimate of total cloud with the IR (BCLE) algorithm, dN_B , depends on the sensitivity of the algorithm to errors in the cloud/no cloud temperature threshold, and the magnitude of this error. The corresponding error formula is

$$dN_B = \frac{\partial N_B}{\partial T_{c/nc}} dT_{c/nc}. \quad (17)$$

As an estimate of the sensitivity of the algorithm to $T_{c/nc}$, we have used results for a total of 230 ocean subtargets observed for one summer and one winter day off the east coast of the United States with two different versions of the BCLE algorithm; version-2, where the $T_{c/nc}$ was consistently 3.48°C warmer than version-4, the final version. The average total cloud amount was 18.9% greater for version-2 than for version-4, which for a 3.48 warmer $T_{c/nc}$, implies a cloud amount sensitivity of 5.4%/°C.

The error in $T_{c/nc}$, consistent with the discussions in sections 3a and 4a, is primarily the result of uncertainty in the amount of atmospheric attenuation, which has

a SD of 2°C, and the uncertainty in the surface temperature, which, as discussed in section 4a, is about 1°C. Thus, if these errors are assumed to be statistically independent (uncorrelated), the error in the IR algorithm estimate of cloud amount is computed to be

$$dN_B = \pm 5.4\%/^{\circ}\text{C} \times 2.2^{\circ}\text{C} = \pm 12.1\%. \quad (18)$$

Of course, this error is related to the amount and type of cloud being observed. For example, if the IR algorithm detects 100% cloud, the cloud types would typically be middle and high in altitude (cf. Fig. 5) with radiative temperatures far removed from the cloud/no cloud threshold. Hence, the IR algorithm error would be considerably smaller. As discussed with reference to TOMS in section 4b(1), it is this reduction in the error of the IR algorithm as cloud altitude and amount increases that led to the particular form of the bispectral merge algorithm (10).

3) NCLE ALGORITHM ERROR COMPUTATIONS

The error formula for the NCLE algorithm (10) is written:

$$dN_N = \frac{\partial N_N}{\partial N_B} dN_B + \frac{\partial N_N}{\partial W} dW + \frac{\partial N_N}{\partial N_T} dN_T. \quad (19)$$

The sensitivity terms (partial derivatives) in (19) are, from differentiation of (10),

$$\frac{\partial N_N}{\partial N_B} = 1 - W; \quad \frac{\partial N_N}{\partial W} = N_T - N_B; \quad \frac{\partial N_N}{\partial N_T} = W \quad (20)$$

and substituting into (19) and factoring gives

$$dN_N = dN_B + W(dN_T - dN_B) + dW(N_T - N_B). \quad (21)$$

In evaluating (21), it is assumed that: the error in the BCLE estimate, dN_B , is given by (18); the error in the weighting factor, dW , is equal to dN_B , since it is determined from the BCLE algorithm (cf. section 3c).

To estimate the error in the NCLE total cloud amount for clear conditions, it is further assumed that: dN_T is 7.9%, the conservative estimate from (16); that W is in error by dW , i.e., $W = W(\text{CLR}) - dW = 1.0(\text{CLR}) - 0.121 = 0.879$; that the errors dN_B and dN_T are statistically independent such that the second term on the rhs of (21) is $W[(dN_T)^2 + (dN_B)^2]^{1/2}$; and that N_T and N_B each depart from clear values of zero by their respective errors. Thus, if the error terms in (21) are allowed to all have the same sign, then the maximum estimate of the error in the NCLE-derived cloud amount for clear conditions is

$$dN_N(\text{CLR}) = 12.1\% + 0.879(7.9^2 + 12.1)^{1/2} + 0.121|7.9 - 12.1| \quad (22)$$

or

$$dN_N(\text{CLR}) = \pm 25.3\%.$$

A more conservative estimate is computed by assuming that the error terms in (21) combine as the sum of squares, which after taking the square root, gives

$$dN_N(\text{CLR}) = \pm 17.6\%. \quad (23)$$

Of course, if N_T and N_B and W are assumed to have the values expected of clear conditions, i.e., 0%, 0%, and 1, respectively, then (21) reduces to the minimum estimate of the error,

$$dN_N(\text{CLR}) = dN_T = \pm 7.9\%. \quad (24)$$

Thus, the NCLE algorithm error for clear conditions is estimated to be in the range between 7.9% and 25.3%.

To evaluate the error at the other cloud amount extreme, overcast, we can assume that: dN_T is 36.6%, again using the conservative estimate from (16); that W is in error by dW , i.e., $W = W(\text{OVC}) + dW = 0.0(\text{OVC}) + 0.121 = 0.121$; that the errors dN_B and dN_T are statistically independent and thus combine as the square root of the sum of squares, as assumed above, and that N_T and N_B each depart from their overcast values of 100% by their respective errors. Thus, if the errors are allowed to all have the same sign in (21), we get for the maximum estimate of the error when conditions are overcast,

$$dN_N(\text{OVC}) = 12.1\% + 0.121(36.6^2 + 12.1)^{1/2} + 0.121|63.4 - 87.9| \quad (25)$$

or

$$dN_N(\text{OVC}) = \pm 19.7\%.$$

The more conservative estimate, if computed as done for clear, is

$$dN_N(\text{OVC}) = \pm 13.3\%. \quad (26)$$

For this case, the minimum estimate of the error in the NCLE-derived cloud amount would be obtained by setting N_T and N_B to 100% and W to 0.0, in (21), giving

$$dN_N(\text{OVC}) = dN_B = \pm 12.1\%. \quad (27)$$

Thus, the probable range in the error of NCLE estimates of overcast conditions would be from 12.1% to 19.7%. The next section will estimate these errors from intercomparisons based on actual satellite data, and hence, should be more representative of the "true" magnitudes of these errors.

c. Validation relative to an analyst

Statistical comparisons between an analyst's estimate derived from independent and concurrent geosynchronous satellite images and conventional meteorological reports and satellite algorithm estimates of cloud amount have been used by Stowe (1984) to estimate the systematic and random errors of the original Nimbus-7 "CLE" cloud product. The slope and intercept of the linear regression line with analyst as dependent

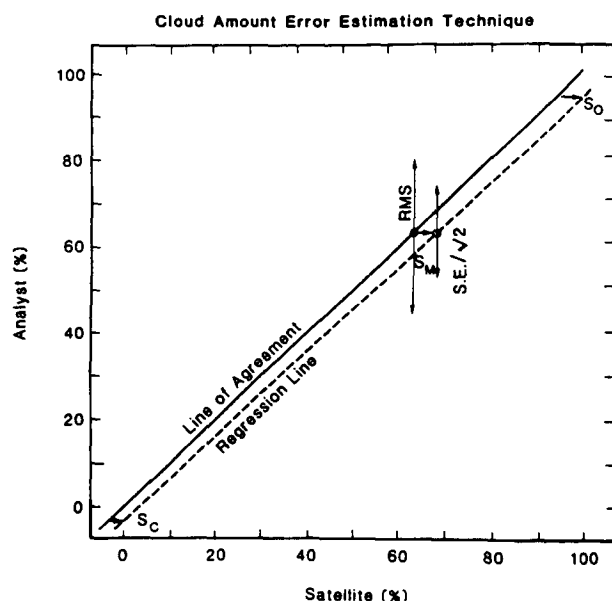


FIG. 8. Schematic illustration of the comparison of Nimbus-7 cloud amount with an analyst's estimates.

variable and satellite as independent variable is used together with the difference in the mean of the two estimates to infer systematic error of the satellite values relative to the analyst. The standard deviation of the random error of the satellite derived cloud amount is assumed to lie between a lower limit given by the standard error of the regression divided by the square root of two and an upper limit given by the RMS difference between analyst and satellite. This same analysis has been used to evaluate the improved Nimbus-7 cloud estimates.

The errors are schematically illustrated in Fig. 8. Depicted on the figure are the line of agreement (or line of perfect fit); the regression line predicting the analyst's estimate from the satellite estimate; three sys-

tematic error estimates given by the difference between the regression line and the line of agreement when, 1) satellite indicates clear, S_C (error when mostly clear), 2) at the mean satellite cloud amount S_M (error at the mean amount), and 3) when the satellite indicates overcast, S_O (error when mostly cloudy); and two estimates of random error, 1) the upper limit, shown as a line whose length is twice the RMS deviation and centered at the analyst's mean amount on the line of agreement, and 2) the lower limit, shown as a line whose length is twice the standard error divided by the square root of two and placed at the mean of both estimates on the regression line.

Tables 3–5 give the results of this validation method for daytime and nighttime selected STAs on 11 June and 3 December 1979 for water, land and coastal areas, respectively. The STAs were located in the eastern third of the United States, western Atlantic ocean and Gulf of Mexico regions. These error estimates are probably larger than the true satellite error because they are computed relative to an analyst, who contributes some systematic and random error to the comparison results which are possibly as large as 10% and 9%–15%, respectively, Stowe (1984).

A substantial reduction in error is evident in both systematic and random error as the information content of the algorithms increases. The large reductions in error between CLE and BCLE for water areas (Table 3) and for land and coastal areas at night (Tables 4 and 5) are the result of using Air Force surface temperatures rather than climatology, which can differ by tens of degrees Celsius for any one day and location, and the improved method of computing the cloud/no cloud thresholds.

Some further reduction in error relative to the analyst is evident between BCLE and NCLE for daytime cases as the TOMS estimate is used in the bispectral algorithm. Daytime land or coastal cases show the least improvement between BCLE and NCLE. For these cases, the TOMS algorithm result is in better agreement with the analyst, but because some of the STAs on

TABLE 3. Errors in Nimbus-7 cloud amounts relative to an analyst for water areas. Plus (minus) means satellite estimate greater (less) than analyst.

Algorithm	Correlation coefficient	Systematic error (%)			Random error (%)	
		Mostly clear	Mean	Mostly cloudy	S.E./ $\sqrt{2}$	RMS
Daytime (230) cases						
IR + Climatology (CLE)	0.74	−5	+11	+22	15	29
IR + Air Force Analysis (BCLE)	0.95	−5	0	+3	8	12
UV Reflectivity (TOMS)	0.92	−8	−2	+2	10	15
Merged IR (BCLE) + UV (TOMS) (NCLE)	0.96	−3	0	+1	8	11
Nighttime (143) cases						
IR + Climatology (CLE)	0.86	−2	+6	+9	12	18
IR + Air Force Analysis (BCLE)	0.95	+1	+4	+5	7	11

TABLE 4. Errors in Nimbus-7 cloud amounts relative to an analyst for land areas. Plus (minus) means satellite estimate greater (less) than analyst.

		Systematic error (%)			Random error (%)		
Algorithm	Correlation coefficient	Mostly clear	Mean	Mostly cloudy	S.E./ $\sqrt{2}$	RMS	
Daytime (127) cases							
IR + Climatology	(CLE)	0.80	-13	-3	11	16	29
IR + Air Force Analysis	(BCLE)	0.81	-19	-14	-5	17	28
UV Reflectivity	(TOMS)	0.87	-10	-6	1	15	22
Merged IR (BCLE) + UV (TOMS)	(NCLE)	0.82	-17	-12	-2	17	27
NCLE for 85 Snow-Free Cases		0.95	-5	-4	-4	10	14
Nighttime (38) cases							
IR + Climatology	(CLE)	0.04	-45	+39	+55	32	63
IR + Air Force Analysis	(BCLE)	0.97	-1	0	+2	8	11

December 3rd are snow covered, the TOMS estimates are not used in determining an NCLE amount. Also, the analyst is possibly confusing some of the snow covered areas with cloudiness, which could explain the apparent systematic underestimation of the satellite estimates relative to the analyst. However, when the comparison is restricted to snow-free cases, the errors for daytime land and coastal areas are greatly reduced and become comparable to the NCLE values for water cases.

The value of TOMS to the bispectral algorithm is better illustrated in the next section, where comparisons will be made with GOES images. From this quantitative analysis, it is concluded that the NCLE (day) and BCLE (night) estimates of cloud amount, when compared with an analyst's estimates derived primarily from independent and concurrent satellite cloud images, have systematic errors less than 10%, random errors ranging between 7% and 16%, and correlation coefficients greater than 0.9, day or night, for snow/ice-free land,

coastal and water areas. Furthermore, these conclusions are consistent with the theoretical results of the previous section, which enhance their credibility.

We have not undertaken the difficult, if not impossible, task of quantitatively validating other than total cloud, as was attempted in Stowe (1984). Since the amounts of low, middle, and high cloud are subject to the particular definition one uses to describe them, it seems more appropriate to validate total cloud. User's who use different definitions of these clouds can use the cloud radiances to place them vertically in the atmosphere. Comparisons with London's (1957) climatology of cloud types are presented and discussed in Part II of this paper.

d. Validation relative to satellite images

Qualitative comparison of Nimbus-7 cloud amount images with GOES (Geosynchronous Observational

TABLE 5. Errors in Nimbus-7 cloud amounts relative to an analyst for coastal areas. Plus (minus) means satellite estimate greater (less) than analyst.

		Systematic error (%)			Random error (%)	
Algorithm	Correlation coefficient	Mostly clear	Mean	Mostly cloudy	S.E./ $\sqrt{2}$	RMS
Daytime (183) cases						
IR + Climatology (CLE)	0.61	−19	+2	+21	20	34
IR + Air Force Analysis (BCLE)	0.72	−26	−13	+6	18	31
UV Reflectivity (TOMS)	0.89	−13	+6	+2	12	19
Merged IR (BCLE) + UV (TOMS) (NCLE)	0.83	−17	−9	−2	14	23
NCLE for 148 Snow-Free Cases	0.91	−8	−4	+2	11	16
Nighttime (93) cases						
IR + Climatology (CLE)	0.71	+10	+25	+31	21	39
IR + Air Force Analysis (BCLE)	0.94	−1	+4	+9	10	14

Environmental Satellite) images has been useful in cloud validation. Figure 9a, b are GOES East visible and infrared images for 1700 UTC 3 December 1979. For comparison, Fig. 10 is a color image of NCLE total cloud amount, mapped for a region similar to the GOES images. The NCLE image is a composite of approximately five orbits with local noon equatorial crossings. Thus, the area around 75°W longitude is coincident in time with the GOES images, far western longitudes are sampled several hours later and far eastern longitudes are sampled several hours earlier. Overall, there is very good agreement in location and amount of cloud between the NCLE total cloud estimates and the GOES images. Examples of good agreement in cloudy areas are from Mexico, extending to the northwestern Atlantic, where clouds associated with a frontal system are composed of many altitude levels (note the ability of the NCLE algorithm to detect the region of broken low altitude cloud at 30°–40°N, 60°–70°W located between two bands of nearly 100% cloud cover); the northern United States from the eastern Pacific to the Great Lakes; from Panama, spreading west to east of Hawaii; the cumulonimbus south of Panama; extended area stratocumulus cloud from the coast of Peru westward into the Pacific to 120°W, associated with subsidence in the subtropical high pressure system; from the west coast of Chile to 130°W; and in the Atlantic, east of Brazil and Argentina. Examples of good agreement in relatively clear areas are a band off the southwest coast of the United States extending northeastward to off the New England coast; the eastern tropical Atlantic ocean; eastern Brazil, on and off the coast; the western part of South America, between 15° and 30°S; the southern equatorial Pacific, north, west and south of the stratocumulus area; and from southern South America off the coast into the Atlantic.

There are, however, several regions where the agreement appears to be only moderately good. The cloudy areas of northeastern South America and the region east of the Andes between the equator and 20°S appear, from the GOES images, to be covered with small-scale cumulus. Many of these clouds may be smaller in size than either the THIR or TOMS FOVs and yet sufficiently developed in the vertical to be cold and bright enough to cause partially filled FOVs to be considered cloud filled by the two respective cloud algorithms. Consequently, the NCLE estimates of cloud amount appear to be too large, by approximately 30%–50%. Also, the relatively clear areas south of Mexico and in the Caribbean and western Atlantic tropical ocean appear to be somewhat too cloudy in the NCLE image. This may be due to either the effects of excessive humidity in these tropical atmospheres or the presence of thin cirrus. Each could cause the affected IR pixels, which in addition may have subpixel cloud within them, to be sufficiently attenuated so as to be classified as middle cloud. This would prevent the TOMS al-

gorithm, which would interpret the expected low reflectance as a small amount of cloud, from reducing the IR estimate for these situations since the TOMS estimate would have little weight due to the cloud being classified as middle [cf. Eq. (10)]. These effects could also contribute to the overestimation apparent in South America.

This illustrates the value of having more than one validation technique. Several geographic locations, exhibit systematic errors that are in excess of the mean errors reported in the previous section. Although differences with the analyst were as large as 50% for a few STAs, the aforementioned locations were essentially outside of the area used for the intercomparison with the analyst.

To illustrate the performance of the three algorithms, BCLE, TOMS, and NCLE, a color image of the differences between NCLE and BCLE total cloud estimates is shown in Fig. 11. It is evident from the image that the majority of the differences between NCLE and BCLE are small, less than 10%. Thus, it is concluded that for most regions, the nighttime estimates of total cloud are going to be comparable in quality to the daytime estimates. However, there are specific situations where the presence of the TOMS reflectance estimates are necessary to get the correct cloud amount or interpretation of cloud type, e.g., thin cirrus.

The regions that are shaded with green to blue colors, are areas where the TOMS reflectance algorithm detected more cloud than the BCLE (IR) algorithm. Clear examples of this are adjacent to the coast of South America, at the Peru–Chile border and in southern Chile, where it is evident from the GOES images that these clouds have very little thermal contrast with the ocean surface, but are quite reflective; and in and around the periphery of the large stratocumulus areas off the Peruvian and south Chilean coasts, extending into the Pacific to about 120°W, where the lack of thermal contrast is exacerbated by edge effects of small element clouds within the THIR FOV.

The pink-to-red colored areas are locations where the TOMS algorithm gave less cloud than the BCLE algorithm. Examples of this are in the regions of northern South America, the Caribbean and South Atlantic oceans, and in the tropical northeastern Pacific Ocean, regions where the NCLE algorithm appears to overestimate cloud amount compared to the GOES images. The TOMS algorithm is compensating for the tendency of the BCLE algorithm to overestimate in these locations, but the NCLE estimates still appear to be too cloudy. Interestingly, the magnitude of the NCLE–BCLE differences when negative is smaller than when the differences are positive, the negative differences never getting more negative than about 30%, except at about 32°N, 43°W. This result can be used to conclude that the IR algorithm rarely detects substantial cloud cover when the scene is clear, but may occasionally detect clear when the scene is mostly cloudy.

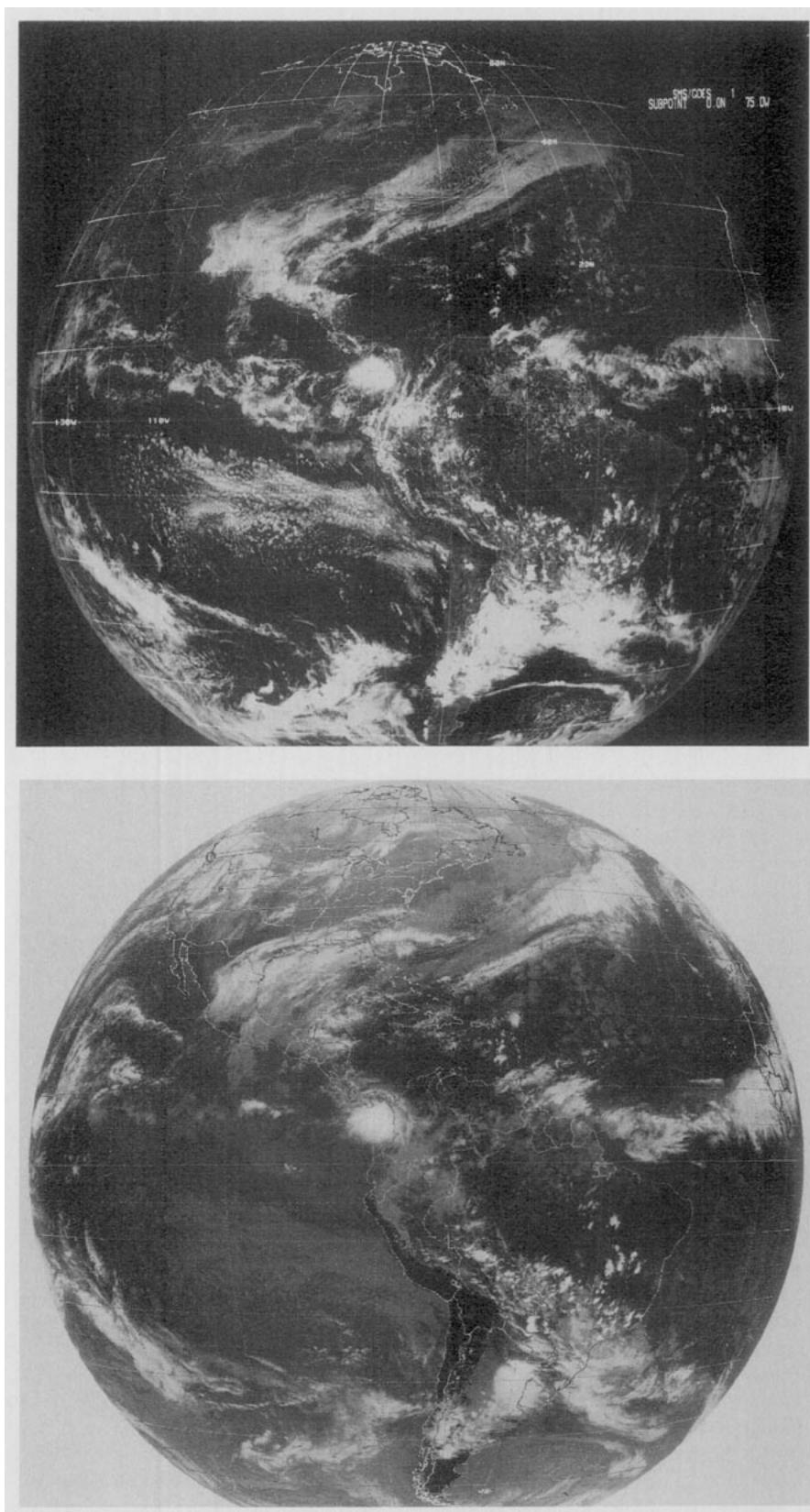


FIG. 9. The GOES east visible (upper) and infrared (lower) images at 1700 UTC 3 December 1979. This is approximately the same time as the Nimbus-7 overpass for the GOES satellite subpoint.

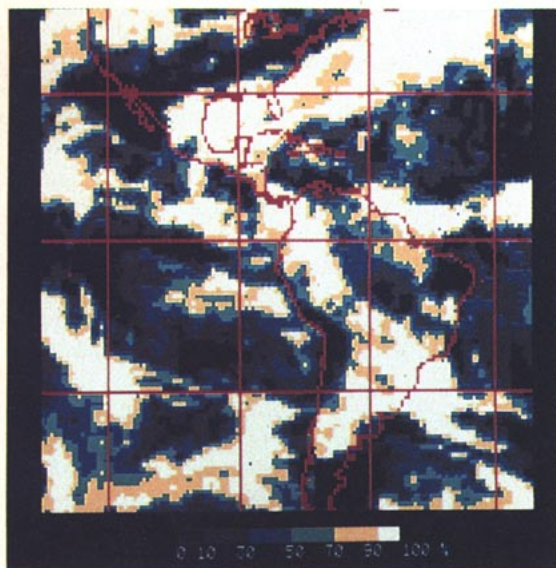


FIG. 10. Map of total cloud amount from the bispectral algorithm (NCLE) near local noon 3 December 1979. The area shown covers most of the area seen in the GOES east images, Figs. 9a, b, for the same day. Note color scale at bottom for cloud amount.

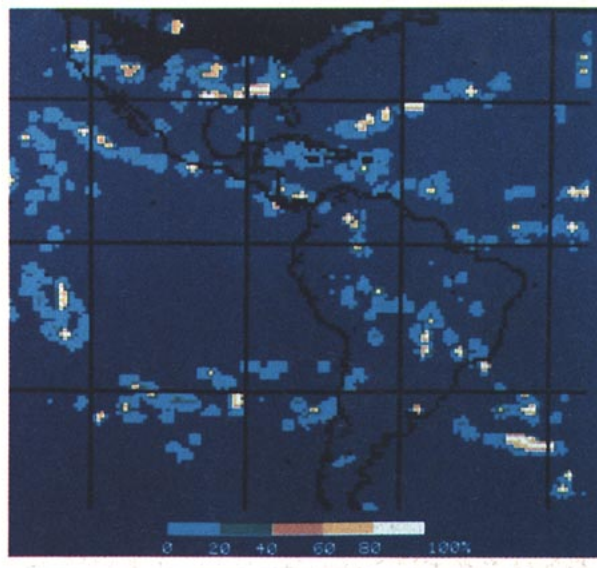


FIG. 12. Map of cirrus cloud amount, which is determined bispectrally, for 3 December 1979. The regions colored black over North America are snow covered areas, where it is not possible to identify cirrus cloud with the bispectral cirrus algorithm.

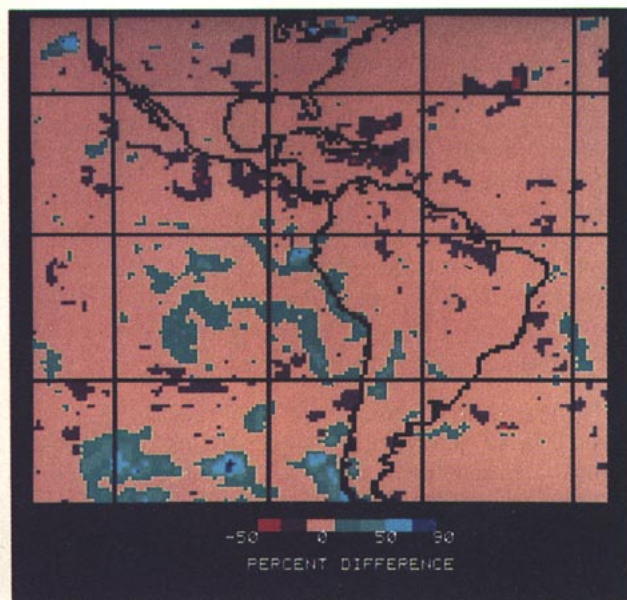


FIG. 11. Map of the difference between the bispectral algorithm (NCLE) total cloud amount and the infrared algorithm (BLCE) total cloud amount (NCLE-BLCE) for 3 December 1979. The color scale at the bottom gives the difference in intervals of 20%.

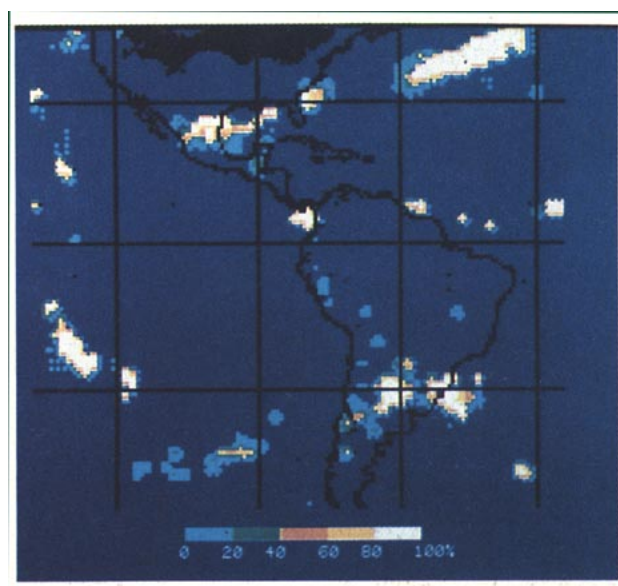


FIG. 13. Map of deep convective clouds for 3 December 1979, as identified bispectrally. As with the cirrus cloud algorithm, it is not possible to detect deep convective cloud over snow and/or ice covered areas, which are shown in black.

From the preceding discussion, it appears that the greatest benefit of using the TOMS cloud estimates is in the detection of low altitude clouds. However, an additional benefit is derived from the use of TOMS for the identification of cirrus and deep convective cloud. Figure 12 shows the location and amount of cirrus cloud as computed from the bispectral cirrus algorithm described in section 3c. The black area in the figure depicts the location of snow. Referring to Figs. 9a and 9b, it is possible to identify cirrus cloud in these images as clouds that are light gray (cold) in the IR image and dark gray (thin) in the visible image. This is the radiative principal upon which the bispectral cirrus algorithm is based. This restricts the detection of cirrus to areas without any underlying (lower altitude) clouds or snow/ice. Comparison of the cirrus amount image with the GOES images shows that the major regions of cirrus evident in the GOES images are indeed detected by the bispectral algorithm. Excellent examples are the band of cirrus which extends from 23°N, 70°W to 35°N, 40°W; the band extending from south Texas through North Carolina, and the region of scattered cirrus in the south Pacific between 25° and 35°S extending from 72° to 120°W.

Because of the form of the bispectral algorithm (10), when low reflectivity cirrus clouds are present, the TOMS will estimate less cloud than BCLE, causing the NCLE estimate to be less than the BCLE value. Thus, some of the negative differences seen in Figure 11 occur at or near regions identified in Fig. 12 as being cirrus. The other negative areas in Fig. 11 are probably the result of errors in the infrared cloud/no cloud threshold caused by humidity. Because of the difficulty in estimating cloud amount for some cloud types such as cirrus, both the BCLE and NCLE estimates of cloud amount are saved in the archive.

It is thus concluded that, although not all cirrus clouds will be detected by the bispectral algorithm, relatively thick (cold) cirrus clouds, not lying over lower level clouds or snow and ice, will be detected by it.

The ability of the bispectral algorithm to detect regions of deep convection is illustrated in Fig. 13. Using the radiative characteristics of deep convective clouds (cumulonimbus) to interpret the GOES images, i.e., pixels that are white (very cold) in the IR and white (very reflective) in the visible, excellent correspondence is seen in the locations of deep convective cloud between Figs. 13 and 9. Of particular value is the ability of the NCLE algorithm to detect the core of cumulonimbus clouds as well as the cirrus shield associated with them. A good example of this is the cumulonimbus system located just south of Panama. Figure 13 shows the location of the core, and Fig. 12 shows the presence of cirrus cloud being advected over the relatively cloud free region to the north. There is one situation that might be mistaken for deep convection. This would occur when cirrus clouds are overlying a multilayered cloud system, as for example, may be

present in the GOES images over the Gulf of Mexico. Some of the other parameters on the NCLE tape, e.g., radiance at 6.7 μm or rms of high cloud radiance at 6.7 and 11.5 μm , might be able to separate deep convection from this multilayered situation.

It is concluded that the locations of deep convection, as derived from the bispectral algorithm, are well correlated with the occurrence of cold and bright clouds on the GOES images, the radiative signature typical of deep convective clouds.

The ability of the NCLE algorithm to detect warm cloud, i.e., cloud whose radiative temperature is greater than the warm cloud/no-cloud threshold [cf. section 3a(5)], has been investigated by qualitative comparison with concurrent and nearby meteorological surface station cloud and radiosonde reports. However, due to the sparsity of surface and raob stations in locations where warm clouds occur, e.g., northern Asia and Canada, we can only conclude that warm clouds are detected by the NCLE algorithm in geographical regions where surface observers frequently report them.

Warm cloud regions found by the algorithm are shown as white areas in Fig. 14a, for 3 December 1979. Warm cloud is most abundant in northeastern Asia, and in Antarctica, with a few areas appearing in northern Canada and Asia. Figure 14b is a computer analysis of warm cloud amount for the same day, showing that, at a resolution of about 1000 km, warm cloud amounts can be quite substantial in the regions where they appear in Fig. 14a. Of course, since over Antarctica, climatological surface temperatures were used [cf. section 4a(1)], and the TOMS reflectance algorithm is inoperative due to snow, the accuracy of the warm cloud amount is uncertain.

The global and seasonal characteristics of the results from the different algorithms and for the different cloud types will be further described in Part II of this paper.

e. Other validation considerations

One important characteristic of satellite cloud estimates is the dependence of these estimates on viewing angle, i.e., satellite zenith angle (SZA). One would desire this dependence to be as near non-existent as possible and whatever dependence does exist, to be a smoothly varying function of SZA. The Nimbus-7 estimates of cloud amount match very well the desired characteristic for SZA dependence, as is seen in Fig. 15, which shows a plot of total amount of cloud estimated with the NCLE algorithm for subtarget areas in December 1979 as a function of SZA. Cloud amount is seen to increase very gradually with increasing SZA, but it does not deviate from the nadir value by more than one percent until SZA exceeds 45 degrees. Using the expression derived by Snow et al. (1985), this gradual dependence on SZA would correspond to the effect expected from a field of cuboidal clouds whose ratio of cloud depth to width was about 0.075. Snow's work

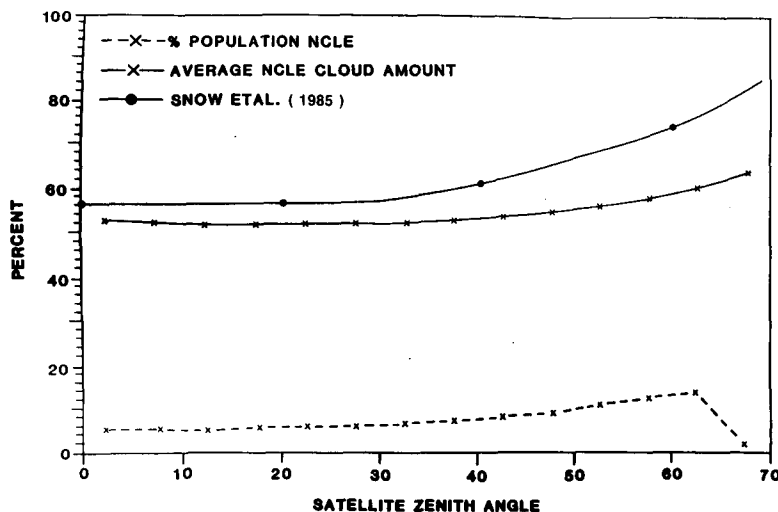


FIG. 15. Nimbus-7 bispectral cloud amount as a function of satellite zenith angle (SZA). Global data for December 1979 are averaged in bins of 5° SZA. The percent of observations in each bin is also plotted. An analysis by Snow et al. (1985) is also shown for comparison.

eraged to target area resolution (CMATRIX) for December 1979. The NCLE and CMATRIX estimates are both seen to vary smoothly over the entire range of cloud amount with a "U" shaped distribution. The much greater occurrence of NCLE estimates of 95%–100%, and to a lesser extent, of 0%–5%, is an indication that the size of overcast and clear areas is more frequently similar to the STA resolution (165 km^2) than to the TA resolution (500 km^2). The greater occurrence at 95%–100% may also be the result of screening large SZA estimates from the CMATRIX TA averages (cf. Table 2). As was shown in Fig. 15, cloud amount estimates do increase with increasing SZA, but they cannot increase beyond 100% cloud amount. This would

then create an artificial population of 100% cloud in the NCLE data distribution, which would occur less frequently in the CMATRIX dataset because of large SZA screening.

5. Summary and conclusions

A global multilevel cloud climatology data archive has been created from an algorithm that uses $11.5 \mu\text{m}$ radiance measurements from the THIR instrument and inferred values of UV reflectivity from the TOMS instrument, both on the Nimbus-7 satellite. This archival is for the interval, April 1979 through March 1985, and includes the parameters of cloud amount in

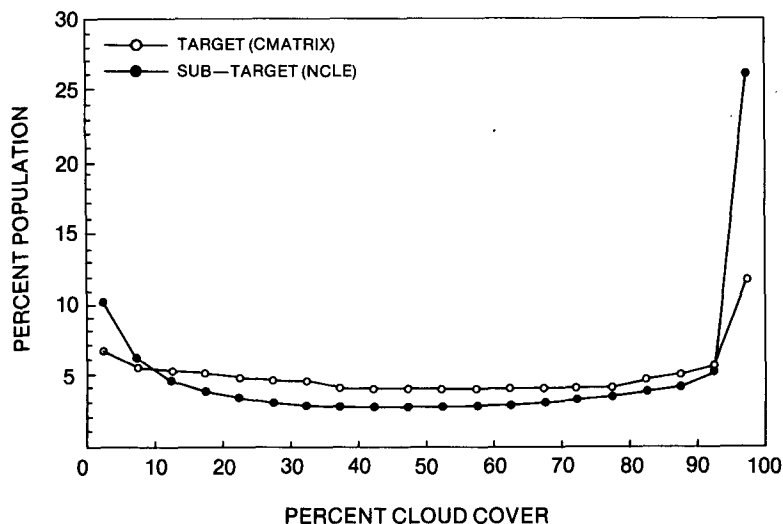


FIG. 16. Histograms of the Nimbus-7 bispectral cloud amount at the subtarget area (165 km^2) and target area (500 km^2) resolutions for December 1979.

three height categories (low, middle, high), cirrus cloud, warm cloud, deep convective cloud, and the radiance of associated cloud tops and of the planet Earth's surface. These parameters, and others that describe the spatial and temporal variability of the cloud parameters, are computed for the ascending (daytime—local noon at the equator) and descending (nighttime—local midnight at the equator) passes of the satellite at the subtarget area (165 km)² and target area (500 km)² resolutions and are averaged daily and monthly. This is sufficient to study diurnal cloud variations about these two times but insufficient for studies of the complete diurnal cycle.

For the sunlit overpasses, two independent estimates of total cloud are made from both a UV and an IR algorithm, which are combined into a composite estimate. The primary reason for using reflectivity measurements in the bispectral algorithm is to aid the IR algorithm in the detection of low altitude clouds, which have very little thermal contrast with the surface. Also they make possible the identification of cirrus and deep convective clouds. For the nighttime overpasses, only the IR algorithm is used.

Various analysis methods have been used to validate the Nimbus-7 cloud algorithms. The following conclusions have been made: 1) the auxiliary information used to estimate the cloud/no-cloud threshold for the THIR IR radiances and to determine whether the TOMS reflectances are affected by snow or ice cover is sufficiently accurate for the purpose of developing a cloud climatology with the Nimbus-7 data; 2) based on a theoretical sensitivity analysis and on an empirical comparison between cloud amount estimated by an analyst, using GOES images and auxiliary meteorological data, and by the Nimbus-7 algorithms, the systematic errors of the Nimbus-7 estimates, relative to the analyst, are less than 10% and the random errors range from 7% to 16%. The errors of the satellite cloud estimates may be lower than these estimates since the analyst contributes systematic and random error to the comparison; 3) the TOMS algorithm rarely causes the bispectral (NCLE) algorithm results to depart by more than 10% from the IR algorithm (BCLE). Thus, the nighttime cloud estimates, which use the IR algorithm solely, should only be slightly less accurate than the daytime estimates, with the exception of geographical regions where low level cloud systems are prevalent, e.g., the west coasts of subtropical continents; 4) from qualitative comparison with GOES cloud images, Nimbus-7 estimates of cirrus and deep convective cloud amounts (daytime only) are reasonable; 5) the Nimbus-7 algorithm is capable of detecting some low altitude clouds when the cloud-top temperatures are warmer than the Earth's surface (warm cloud); and 6) the Nimbus-7 cloud amount estimates are weakly dependent on satellite zenith angle and the frequency distribution of cloud amount is "U"-shaped and varies smoothly from 0% to 100%.

The Nimbus-7 cloud climatology archive meets the requirements for many studies of climate modeling and diagnosis and also for studies related to the earth radiation budget. The existence of data covering the same time period from the Earth Radiation Budget (ERB) instrument, also aboard the Nimbus-7 satellite, provides a unique opportunity for the study of the interaction of clouds and the radiation budget for a period of six years, which includes the major El Niño event of 1982–83.

Acknowledgments. We greatly appreciate the help offered by Messrs. V. R. Taylor and R. F. Ryan, NOAA/NESDIS, who prepared some of the figures for this paper. We also thank E. Hurley and A. Fleig of NASA/GSFC and G. Esenwein of NASA HQ for their support and encouragement of our work on the Nimbus-7 cloud dataset. One of the authors (LLS) is also indebted to P. K. Rao, G. Ohring, and A. Gruber of NOAA/NESDIS and E. Epstein of NOAA/NWS, for their support and encouragement during the many years spent on this project. We would also like to thank Brenda Vallette of Research and Data Systems Corporation for her help in preparing and editing the revised manuscript.

REFERENCES

- Ashburn, E. V., and R. G. Weldon, 1956: Spectral diffuse reflectance of desert surfaces. *J. Opt. Soc. Amer.*, **46**, 583–586.
- Barkstrom, B. R., 1984: The earth radiation budget experiment (ERBE). *Bull. Amer. Meteor. Soc.*, **65**, 1170–1185.
- Beers, Yardley, 1958: *Introduction to the Theory of Error*. Addison-Wesley, 66 pp.
- Berlyand, T. G., and L. A. Strokina, 1980: Global distribution of total cloud amount. *Gidrometeoizdata*, S. Warren, Trans. Leningrad, 18 pp.
- Brower, R. L., H. S. Gorbard, W. G. Pichel, T. L. Signore and C. Walton, 1976: Satellite derived sea-surface temperatures from NOAA spacecraft, Tech. Memo. NESS 78, NOAA, Washington, DC, 74 pp.
- Cebula, R. P., H. Park and D. F. Heath, 1987: Characterization of the Nimbus-7 SBUV radiometer for the long-term monitoring of stratospheric ozone. *J. Atmos. Oceanic Technol.*, **5**, 215–227.
- Cess, R. D., B. P. Briegleb and M. S. Lian, 1982: Low-latitude cloudiness and climate feedback: comparative estimates from satellite data. *J. Atmos. Sci.*, **39**, 53–59.
- Coakley, J. A., 1987: A dynamic threshold method for obtaining cloud cover from satellite imagery data. *J. Geophys. Res.*, **92**(D4), 3985–3990.
- , and F. P. Bretherton, 1982: Cloud cover from high-resolution scanner data: Detecting and allowing for partially filled fields-of-view. *J. Geophys. Res.*, **87**(C7), 4917–4932.
- Coulson, K. L., and D. W. Reynolds, 1971: The spectral reflectance of natural surfaces. *J. Appl. Meteor.*, **10**, 1285–1295.
- Dave, J. V., 1964: Meaning of successive iteration of the auxiliary equation in the theory of radiative transfer. *Astrophys. J.*, **140**, 1292–1303.
- Eck, T. F., P. K. Bhartia, P. H. Hwang and L. L. Stowe, 1987: Reflectivity of earth's surface and clouds in ultraviolet from satellite observations. *J. Geophys. Res.*, **92**(D4), 4287–4296.
- Fleig, A. J., K. F. Klenk, P. K. Bhartia and D. Gordon, 1982: User's guide for the total-ozone mapping spectrometer (TOMS) instrument first-year ozone-T data set. NASA Ref. Publ. 1096, 43 pp.
- Fritz, S., and P. K. Rao, 1967: On the transmission through cirrus

- clouds and the estimation of relative humidity from satellites. *J. Appl. Meteor.*, **6**, 1088–1096.
- Fye, F. K., 1978: AFGWC automated cloud analysis, T.M. 78-002, Global Weather Central, Offutt AFB, 97 pp.
- Gordon, C. T., R. D. Hovaneec and W. F. Stern, 1984: 3D-Neph and surface observation-analyses of monthly mean cloudiness and their influence upon model-diagnosed radiative fluxes. *J. Geophys. Res.*, **89**(D3), 4713–4738.
- Goward, S. N., G. D. Cruickshanks and A. S. Hope, 1985: Observed relation between thermal emission and reflected spectral radiance of a complex vegetated landscape. *Remote Sens. Environ.*, **18**, 137–146.
- Griggs, M., 1968: Emissivities of natural surfaces in the 8- to 14-micron spectral region. *J. Geophys. Res.*, **73**, 7545–7551.
- Hartmann, D. L., and D. A. Short, 1980: On the use of earth radiation budget statistics for studies of clouds and climate. *J. Atmos. Sci.*, **37**, 1233–1250.
- Hahn, C. J., S. G. Warren, J. London, R. M. Chervin and R. Jenne, 1982: *Atlas of Simultaneous Occurrence of Different Cloud Types Over the Ocean*, NCAR Tech. Note TN-201 + STR, 212 pp.
- , —, —, and —, 1984: *Atlas of Simultaneous Occurrence of Different Cloud Types Over Land*, NCAR Tech. Note TN-241 + STR, 214 pp.
- Heath, D., A. J. Krueger, and H. Park, 1978: The solar backscatter ultraviolet (SBUV) and total ozone mapping spectrometer (TOMS) experiment. *The Nimbus-7 User's Guide*, C. R. Madrid, Ed., NASA, Goddard Space Flight Center, 175–211.
- Hughes, N. A., and A. Henderson-Sellers, 1985: Global 3D-Neph-analysis of total cloud amount: Climatology for 1979. *J. Climate Appl. Meteor.*, **24**, 7, 669–686.
- Hwang, P. H., Ed., 1982: *Nimbus-7 temperature humidity infrared radiometer (THIR) data user's guide*. NASA/Goddard Space Flight Center, 52 pp.
- Jacobowitz, H., H. V. Soule, K. L. Kyle, F. D. House and the Nimbus-7 ERB Experiment Team, 1984: The earth radiation budget (ERB) experiment: An overview. *J. Geophys. Res.*, **89**(D4), 5021–5038.
- Jenne, R. L., H. L. Crutcher, H. van Loon and J. J. Taljaard, 1974: A selected climatology of the southern hemisphere: Computer methods and data availability. Tech. Note NCAR-TN/STR-92, Boulder, CO., 91 pp.
- London, J., 1957: A study of the atmospheric heat balance. Final Report, Contract AF 19(122)-165 Department of Meteorology and Oceanography, College of Engineering, New York University, 99 pp. [AF CFC-TR-57-287.]
- Lucas, S. A., S. J. Hall and J. D. Mortens, 1975: The AFGWC snow cover analysis model, AFGWC Tech. Memo. 75-1, HQ Air Force Global Weather Central, Offutt AFB, 19 pp.
- Nieuwenhuis, G. J. A., E. H. Smidt and H. A. M. Thunnissen, 1985: Estimation of regional evapotranspiration of arable crops from thermal infrared images. *Int. J. Remote Sens.*, **6**, 1319–1334.
- Ohring, G., P. F. Clapp, T. R. Headdinghouse and A. F. Kruger, 1981: The quasi-global distribution of the sensitivity of the earth-atmosphere radiation budget to clouds. *J. Atmos. Sci.*, **2539**–2541.
- Ostle, B., and R. W. Mensing, 1975: *Statistics in Research*, Iowa State University Press, 596 pp.
- Schiffer, R. A., and W. B. Rossow, 1983: The international satellite cloud climatology project: The first project of the world climate research program. *Bull. Amer. Meteor. Soc.*, **64**, 779–784.
- Slingo, J., 1987: The development and verification of a cloud prediction scheme for the ECMWF model. *Quart. J. Roy. Meteor. Soc.*, **113**, 899–927.
- Smith, E. A., 1984: Radiative forcing of the southwest summer monsoon (a satellite perspective). Ph.D. thesis, Colorado State University, ASP 383, 520 pp.
- Smith, J. A., 1983: Matter-energy interaction in the optical region, *ASP Manual of Remote Sensing*, Vol. 1, 2nd ed., Falls Church.
- Snow, J. W., J. T. Bunting, R. P. Entremont, R. D. Grantham and K. R. Hardy, 1985: Space shuttle cloud photographs assist in connecting meteorological satellite data. *Eos*, **489**–490.
- Stowe, L. L., 1984: Evaluation of Nimbus-7 THIR/CLE and Air Force 3-D nephanalysis estimates of cloud amount. *J. Geophys. Res.*, **89**(D4), 5370–5380.
- , P. P. Pellegrino, P. H. Hwang, P. K. Bhartia, T. F. Eck, C. S. Long, L. G. Wellemeier and H. Y. M. Yeh, 1986: Spatial and temporal characteristics of global cloud cover as observed from the Nimbus-7 satellite. *Sixth Conf. on Atmospheric Radiation*, Boston, Amer. Meteor. Soc. 99–102.
- WCRP, 1982: The international satellite cloud climatology project (ISSCP) preliminary implementation plan. Rev. 1, WCP-35.
- Wetherald, R. T., and S. Manabe, 1980: Cloud cover and climate sensitivity. *J. Atmos. Sci.*, **37**, 1485–1510.
- WMO, 1956: *International Cloud Atlas*, Vol. 1, World Meteor. Organization, Geneva.
- , 1978: *JOC Study Conf. on Parameterization of Extended Cloudiness and Radiation for Climate Models*, Oxford, GARP Climate Dyn. Subprogram, Geneva.